

# Solving the Constrained Random Disambiguation Path Problem via Lagrangian Relaxation and Graph Reduction

Li Zhou\* & Elvan Ceyhan\*

## Contents

<b>1</b>	<b>Introduction</b>	<b>3</b>
<b>2</b>	<b>Problem Formulation</b>	<b>4</b>
2.1	Formulating RCDP as a Weight-Constrained Shortest Path Problem . . . . .	5
2.2	Risk Modeling and Surrogate Cost Approximation . . . . .	6
2.3	Graph Initialization with Risk and Resource Embedding . . . . .	8
<b>3</b>	<b>COLOGR: A Lagrangian &amp; Graph-Reduction Framework</b>	<b>9</b>
3.1	Path Planning Using Lagrangian Relaxation . . . . .	9
3.2	Two-Phase Vertex Elimination . . . . .	10
3.3	COLOGR: Combining TPVE & Lagrangian Search . . . . .	12
3.4	Guarantees and Complexity of COLOGR . . . . .	13
<b>4</b>	<b>Design and Analysis of the RCDP Traversal Policy</b>	<b>17</b>
4.1	Algorithmic Framework . . . . .	18
4.2	Theoretical Guarantees and Benchmark Comparison . . . . .	18
4.3	Illustrative Example . . . . .	20
<b>5</b>	<b>Empirical Evaluation via Monte Carlo Simulation</b>	<b>20</b>
5.1	Simulation Design and Experimental Setup . . . . .	21
5.2	Performance Comparison . . . . .	22
5.3	Summary of Key Empirical Findings . . . . .	26
5.4	Evaluation of Policy Robustness . . . . .	26
<b>6</b>	<b>Discussion and Conclusions</b>	<b>27</b>
	<b>A1Pseudocode for COGR and LOGR Algorithms</b>	<b>29</b>

---

\*Department of Mathematics and Statistics, Auburn University, Auburn, AL 36849, USA  
 emails: lzz0062@auburn.edu (corresponding author), ceyhan@auburn.edu

<b>A2</b>	<b>Proofs of Main Theoretical Results</b>	<b>30</b>
A2.1	Cut-Based Cost Bounds . . . . .	30
A2.2	Identification Results under Lagrangian Ambiguity . . . . .	31
A2.3	Spurious Dual Optima Vanish under High RBG . . . . .	33
A2.4	Theorems and Propositions in Section 4.2 . . . . .	33
<b>A3</b>	<b>Tuning the Scaling Parameter <math>\alpha</math> in the Linear Undesirability Function</b>	<b>34</b>
A3.1	Convergence to the Benchmark under Perfect Sensor Precision . . . . .	35
<b>A4</b>	<b>Details of the Monte Carlo Simulations</b>	<b>36</b>
A4.1	Graph Reduction Performance: TPVE vs. SNE . . . . .	36
A4.2	Comprehensive Comparisons of Traversal Policies . . . . .	37
A4.3	Efficacy of the Bayesian Linear Undesirability Function . . . . .	43
A4.3.1	Sensitivity to the Proportion of True Obstacles . . . . .	43
A4.3.2	Impact of Sensor Accuracy on Traversal Cost . . . . .	44
A4.3.3	Effect of Obstacle Spatial Pattern on Pathfinding Performance . . . . .	45
A4.4	Visualization of Relative Efficiency . . . . .	46

**Abstract**

We study a resource-constrained variant of the Random Disambiguation Path (RDP) problem, a generalization of the Stochastic Obstacle Scene (SOS) problem, in which a navigating agent must reach a target in a spatial environment populated with uncertain obstacles. Each ambiguous obstacle may be disambiguated at a (possibly heterogeneous) heterogeneous resource cost, subject to a global disambiguation budget. We formulate this constrained planning problem as a Weight-Constrained Shortest Path Problem (WCSPP) with risk-adjusted edge costs that incorporate probabilistic blockage and traversal penalties. To solve it, we propose a novel algorithmic framework—COLOGR—combining Lagrangian relaxation with a two-phase vertex elimination (TPVE) procedure. The method prunes infeasible and sub-optimal paths while provably preserving the optimal solution, and leverages dual bounds to guide efficient search. We establish correctness, feasibility guarantees, and surrogate optimality under mild assumptions. Our analysis also demonstrates that COLOGR frequently achieves zero duality gap and offers improved computational complexity over prior constrained path-planning methods. Extensive simulation experiments validate the algorithm’s robustness across varying obstacle densities, sensor accuracies, and risk models, consistently outperforming greedy baselines and approaching offline-optimal benchmarks. The proposed framework is broadly applicable to stochastic network design, mobility planning, and constrained decision-making under uncertainty.

**Keywords:** Stochastic obstacle scene; Resource-constrained path planning; Lagrangian duality; Risk-aware navigation; Vertex elimination; Sensor uncertainty

# 1 Introduction

Graph-based navigation in stochastic and partially observable environments is a fundamental problem in autonomous systems, with applications ranging from mobile robotics and autonomous driving to coordinated multi-agent systems and GNSS-denied navigation. These environments are often characterized by incomplete, noisy, or dynamically evolving information, necessitating robust path planning under uncertainty. In response, a diverse body of research has emerged, including approaches based on greedy heuristics (Aksakalli et al., 2011; Aksakalli and Ari, 2014), reinforcement learning in partially observable settings (Zweig et al., 2020), and probabilistic planning via factor graphs for GNSS/INS fusion (Xin et al., 2023), among others.

Several classical formulations have laid the foundation for modern stochastic path planning. The *Stochastic Obstacle Scene (SOS)* problem (Papadimitriou and Yannakakis, 1991) models environments populated with probabilistic obstacles whose true blockage is unknown prior to traversal. The *Random Disambiguation Path (RDP)* problem (Priebe et al., 2005) extends this setting by introducing a disambiguation mechanism: upon encountering a potentially obstructing region (e.g., an obstacle), a navigating agent (NAVA) may resolve its status—blocking or non-blocking—at the cost of a disambiguation action. The goal is to minimize expected traversal cost, balancing movement and information acquisition.

In the RDP framework, the environment consists of disk-shaped obstacles, each either truly blocking or not. Their status is inferred probabilistically from a noisy sensor model. The NAVA may choose to disambiguate an obstacle upon contact, incurring a nonzero cost. Existing policies typically assign approximate expected costs to edges and use shortest path algorithms such as Dijkstra’s algorithm (Dijkstra, 1959) to compute traversal plans. Examples include Reset Disambiguation (RD) (Aksakalli et al., 2011), Distance-to-Termination (DT), and other penalty-based policies (Aksakalli and Ari, 2014; Alkaya et al., 2021), which differ in how they account for obstacle interactions. These approaches, while effective in certain settings, do not explicitly model realistic limitations on disambiguation resources.

In practice, such actions often incur heterogeneous costs and are subject to cumulative resource constraints. For instance, in automated logistics, a fleet vehicle must avoid traffic blockages under limited fuel or energy reserves; in disaster response, a medical team may need to verify road access to clinics with limited communication capabilities; and in minefield navigation, an autonomous agent may be constrained by a finite supply of detection scans. In such cases, methods that restrict only the *number* of disambiguations (Fishkind et al., 2007; Alkaya and Algin, 2015; Yildirim et al., 2019) fall short, as they fail to account for continuous resource consumption and variable disambiguation costs.

To address these shortcomings, we propose a resource-aware extension of the RDP framework. We formulate the *RDP with Constrained Disambiguation (RCDP)* problem as a *Weight Constrained Shortest Path Problem (WCSP)*, where the objective is to minimize traversal cost subject to a global constraint on disambiguation expenditure. This formulation captures both uncertainty in obstacle fields and cumulative limitations on information acquisition resources.

We develop a novel RCDP traversal policy that leverages probabilistic sensor information through risk-sensitive cost approximations, enabling more accurate estimation under disambiguation. Our method embeds the constrained optimization problem into a Lagrangian relaxation framework, augmented with multiple graph reduction steps that eliminate infeasible paths, reduce problem dimensionality, and ensure optimality by closing the duality gap. Unlike previous

methods that use static or greedy cost assignment, our algorithm dynamically adapts to resource restrictions and maintains feasibility with respect to the disambiguation budget.

In addition to addressing core challenges in stochastic path planning, our framework connects naturally to related work in network interdiction (Israeli and Wood, 2002; Smith and Song, 2020), particularly in settings where uncertainty and partial observability influence adversarial interactions (Azizi and Seifi, 2024; Sadeghi and Seifi, 2024). However, the RCDP problem focuses on the navigator’s decision-making process rather than the interdictor’s, making it a distinct yet complementary contribution to the broader literature on constrained decision-making in uncertain networks.

The remainder of this paper is structured as follows. Section 2 formally defines the RCDP problem, introducing modeling assumptions, cost structures, and risk measures. Section 3 presents the COLOGR optimization algorithm, which combines Lagrangian relaxation with a two-phase graph reduction scheme. Section 4 details the RCDP traversal policy, including its implementation and theoretical guarantees. Section 5 reports empirical results from extensive Monte Carlo simulations under varying obstacle and sensor conditions. Section 6 concludes with a summary and directions for future research. Appendix Section contains algorithmic pseudocode and proofs for the main theoretical results, and also provides additional technical content omitted for brevity, including secondary proofs,  $\alpha$ -sensitivity analysis, a Bayesian LU extension, and extended simulation results.

## 2 Problem Formulation

We introduce a resource-constrained extension of the *Random Disambiguation Path* (RDP) problem, a probabilistic path planning framework originally proposed by Priebe et al. (2005), which builds on the foundational *Stochastic Obstacle Scene* (SOS) problem of Papadimitriou and Yannakakis (1991). In this setting, a navigating agent (NAVA) must traverse from a source location  $s$  to a target location  $t$  within a bounded planar domain  $\Omega \subset \mathbb{R}^2$  that contains a set of spatially distributed disk-shaped obstacles whose true statuses—blocking or non-blocking—are initially unknown.

Let  $X = X_T \cup X_F$  denote the set of obstacle centers, partitioned into true obstacles  $X_T$  that block traversal and false obstacles  $X_F$  that permit passage. Each obstacle  $x \in X$  is modeled as a closed disk of fixed radius  $\text{radius}(x) > 0$  centered at  $x$ . The agent does not know an obstacle’s status a priori but instead receives a probabilistic estimate from a noisy sensor, represented by a function  $\pi : X \rightarrow [0, 1]$ , where  $\pi_x := \pi(x)$  denotes the probability that obstacle  $x$  is truly blocking. Obstacle statuses are assumed to be independent and remain static throughout the traversal.

Upon reaching the boundary of an ambiguous obstacle  $x$ , the NAVA may pay a disambiguation cost  $\delta_x > 0$  to reveal its true status. If  $x$  is non-blocking, the agent proceeds; otherwise, it must reroute. Each disambiguation action consumes a portion of a cumulative resource budget, such as time, energy, or computational capacity. The goal is to minimize the expected total cost, comprising both traversal and disambiguation expenditures, while respecting this global constraint.

To make the problem computationally tractable, we discretize  $\Omega$  using an 8-adjacency integer lattice, transforming the continuous domain into a finite undirected graph  $G = (V, E)$ .

Each vertex  $v \in V$  corresponds to a lattice point with integer coordinates  $(i, j)$ , and each edge  $e \in E$  connects adjacent vertices horizontally, vertically, or diagonally. The edge length  $\ell_e$  equals the Euclidean distance between its endpoints. This discretization balances representational fidelity with computational efficiency. As discussed in Remark 2.1, finer grids offer greater path redundancy but also increase problem size and complexity due to more frequent obstacle-edge intersections.

An edge  $e \in E$  is traversable if it does not intersect any true or unresolved obstacle. If it intersects an ambiguous obstacle, the agent may disambiguate it at one of the edge’s endpoints before traversal. Let  $p$  denote a valid  $s$ - $t$  path in  $G$ , and let  $\mathcal{C}_p$  denote the total (random) cost incurred along  $p$ , which includes both traversal distance  $\ell_p$  and disambiguation cost  $\delta_p$ :

$$\mathcal{C}_p = \ell_p + \delta_p,$$

where  $\ell_p$  is the sum of edge lengths along  $p$ , and  $\delta_p = \sum_{x:p \cap D(x) \neq \emptyset} \delta_x$  is the total cost of disambiguating all ambiguous obstacles intersected by  $p$ .

Let  $\mathcal{P}(s, t)$  denote the set of all feasible paths from  $s$  to  $t$  in  $G$ . The objective is to find a path  $p \in \mathcal{P}(s, t)$  that minimizes the expected total cost:

$$\min_{p \in \mathcal{P}(s, t)} \mathbf{E}[\mathcal{C}_p].$$

This optimization accounts for both obstacle uncertainty and the cost trade-offs induced by disambiguation.

**Remark 2.1.** *The granularity of the spatial discretization strongly influences both the computational complexity and robustness of the path planning model. Specifically, a finer grid increases the number of vertices and edges, expanding the feasible solution space and allowing more alternative paths between  $s$  and  $t$ . This enhances resilience to disruptions, as measured by the local vertex connectivity  $\kappa(s, t)$ —the minimum number of vertices whose removal disconnects  $s$  from  $t$  in  $G$ . A higher  $\kappa(s, t)$  implies greater robustness against obstacle insertions or adversarial interference. However, increased connectivity also raises combinatorial complexity, as the number of feasible paths and potential disambiguation points grows rapidly.  $\square$*

In the Discrete RDP (D-RDP) model, the vertex closest to the source is selected as  $s$ , and the closest to the target is designated  $t$ . The cost  $\mathcal{C}_p$  is inherently stochastic due to random obstacle locations and uncertain statuses. The RDP formulation minimizes its expected value, and in the constrained variant introduced in Section 2.1, this optimization is carried out under a global disambiguation budget, yielding a tractable yet flexible framework for risk-aware path planning in uncertain environments.

## 2.1 Formulating RCDP as a Weight-Constrained Shortest Path Problem

We now formalize the *Random Constrained Disambiguation Path* (RCDP) problem as a constrained optimization framework. In this extension, the navigating agent (NAVA) operates under a global disambiguation budget  $\delta_{\max}$ , representing the maximum allowable cost for resolving obstacle statuses along the path. The objective is to find a feasible path  $p$  from the source  $s$  to the destination  $t$  that minimizes the expected total cost, while ensuring the total disambiguation expenditure does not exceed  $\delta_{\max}$ .

This yields the following constrained optimization problem:

$$\min_{p \in \mathcal{P}(s,t)} \mathbf{E}[\mathcal{C}_p] \quad \text{subject to} \quad \delta_p \leq \delta_{\max}, \quad (1)$$

which is a specific instance of the classical *Weight Constrained Shortest Path Problem* (WCSPP), with the “weight” corresponding to cumulative disambiguation cost.

We consider two cost structures for disambiguation. In the *uniform model*, all obstacles incur a fixed cost  $\delta_x = \delta$  for every  $x \in X$ . In contrast, the *heterogeneous model* allows  $\delta_x$  to vary based on contextual factors such as sensor reliability, terrain conditions, or distance to the goal.

## 2.2 Risk Modeling and Surrogate Cost Approximation

Computing the exact expected cost  $\mathbf{E}[\mathcal{C}_p]$  for a path  $p$  is generally intractable due to the exponential number of possible obstacle realizations. To enable efficient planning under uncertainty, we adopt a surrogate cost approximation based on deterministic edge-level penalties.

Specifically, we replace  $\mathbf{E}[\mathcal{C}_p]$  with an additive deterministic surrogate:

$$\tilde{\mathcal{C}}_p := \sum_{e \in E(p)} (\ell_e + r_e), \quad (2)$$

where  $\ell_e$  is the Euclidean length of edge  $e$ , and  $r_e$  is a penalty term that accounts for the expected disambiguation cost and traversal risk induced by ambiguous obstacles intersecting  $e$ .

This surrogate formulation supports efficient constrained optimization and naturally incorporates sensor-driven uncertainty into edge costs, allowing for scalable planning in environments with limited information and resource constraints.

### Surrogate Constrained Optimization

Combining the deterministic risk-adjusted cost formulation with the disambiguation constraint leads to the following approximation of the RCDP problem:

$$\min_{p \in \mathcal{P}(s,t)} \tilde{\mathcal{C}}_p \quad \text{subject to} \quad \delta_p := \sum_{e \in E(p)} \delta_e \leq \delta_{\max}, \quad (3)$$

where  $\delta_e$  is the surrogate disambiguation cost assigned to edge  $e$ , and  $\delta_p$  is the total accumulated cost over path  $p$ . This formulation maintains the structure of a *Weight Constrained Shortest Path Problem* (WCSPP) and allows for specialized solution techniques. It strikes a balance between computational efficiency and sensitivity to uncertainty, enabling scalable, resource-aware navigation under stochastic conditions.

The algorithmic solution to (3), including graph pruning and Lagrangian dual methods, is developed in Section 3.

### Edge-Level Risk Aggregation

For each edge  $e \in E$ , let  $X_e := \{x \in X : D(x) \cap e \neq \emptyset\}$  denote the set of ambiguous obstacles intersecting the edge. Each obstacle  $x \in X_e$  contributes a risk penalty  $r_x$  and a disambiguation

cost  $\delta_x$ , which are symmetrically divided across intersecting edges since disambiguation may be initiated from either endpoint. Accordingly, we define the edge-level quantities as:

$$r_e := \frac{1}{2} \sum_{x \in X_e} r_x, \quad \delta_e := \frac{1}{2} \sum_{x \in X_e} \delta_x.$$

The value  $r_x$  reflects the perceived risk of traversing near obstacle  $x$  without resolving its status. These edge-level terms enter directly into both the surrogate cost objective and the disambiguation budget constraint. Depending on the sensor model and obstacle features, various forms of  $r_x$  can be adopted from the literature to capture uncertainty and criticality.

### Risk Function Models

We now describe several obstacle-level risk functions  $r_x$  used in the surrogate edge cost formulation. Each function maps the disambiguation cost  $\delta_x$  and the sensor-assigned probability  $\pi_x$  of an obstacle being true to a penalty that reflects the traversal risk associated with ambiguous obstacles. These models, adapted from prior literature, capture different attitudes toward uncertainty and spatial exposure, and they influence how conservative or exploratory the resulting path will be.

**Reset Disambiguation (RD).** The RD model (Aksakalli et al., 2011) defines the risk as:

$$r_x^{\text{RD}} = \frac{\delta_x}{1 - \pi_x}.$$

This function penalizes obstacles more heavily as  $\pi_x \rightarrow 1$ , encouraging early disambiguation of high-risk regions. It represents a pessimistic cost expectation under a greedy traversal policy and provides sharp risk separation for ambiguous areas.

**Distance-to-Termination (DT).** The DT model (Aksakalli and Ari, 2014) incorporates spatial proximity to the goal:

$$r_x^{\text{DT}} = \delta_x + \left( \frac{d(x, t)}{1 - \pi_x} \right)^{-\log(1 - \pi_x)},$$

where  $d(x, t)$  is the Euclidean distance between obstacle  $x$  and the target  $t$ . The formulation emphasizes obstacles near the goal whose status is uncertain, increasing the risk penalty nonlinearly as  $\pi_x$  rises and  $d(x, t)$  shrinks.

**Linear Undesirability (LU).** The LU model (Fishkind et al., 2007) uses a logarithmic transformation to model increasing risk aversion:

$$r_x^{\text{LU}} = -\alpha \log(1 - \pi_x),$$

where  $\alpha > 0$  is a tunable parameter. Larger values of  $\alpha$  induce more conservative routing. We consider three instantiations:

- $r_{15}^L$ : moderate aversion with  $\alpha = 15$ ,
- $r_{30}^L$ : high-risk aversion with  $\alpha = 30$ ,

$r_\delta^L$ : adaptive penalty with  $\alpha = \delta_x$ .

This family provides smooth control over risk sensitivity and avoids unbounded penalties near  $\pi_x = 1$ , making it useful for calibrated trade-offs between caution and efficiency.

These risk models define the edge-wise surrogate cost structure that supports optimization under the disambiguation constraint. Their integration into the RCDP solution process is discussed in Section 3.

### 2.3 Graph Initialization with Risk and Resource Embedding

Before solving the constrained problem in Equation (3), we preprocess the traversal graph  $G = (V, E)$  to assign deterministic edge-level costs and disambiguation weights. This transformation aggregates obstacle-level information into edge-level quantities, thereby enabling efficient constrained shortest path computation.

For each edge  $e \in E$ , let  $X_e := \{x \in X : D(x) \cap e \neq \emptyset\}$  be the set of ambiguous obstacles intersecting  $e$ . Using a selected risk function (e.g., RD, DT, or LU from Section 2.1), we compute:

$$\tilde{\mathcal{C}}_e := \ell_e + r_e, \quad \text{where} \quad r_e = \frac{1}{2} \sum_{x \in X_e} r_x,$$

and assign the edge-level disambiguation weight as:

$$\delta_e := \frac{1}{2} \sum_{x \in X_e} \delta_x,$$

with  $\ell_e$  denoting the Euclidean length of edge  $e$ . The factor 1/2 reflects symmetric allocation since disambiguation can occur from either endpoint.

The initialization process is summarized in Algorithm 1, which takes as input the graph structure, obstacle configuration, sensor probabilities  $\pi_x$ , disambiguation costs  $\delta_x$ , and a specified risk function. The output is an adjusted graph with edge-wise costs and weights that embed both geometric and probabilistic features.

---

#### Algorithm 1 Graph Initialization (GI)

---

**Input:** Graph  $G = (V, E)$ ; obstacles  $X$ ; sensor probabilities  $\pi_x$ ; disambiguation costs  $\delta_x$ ; risk function  $r_x$

**Output:** Adjusted graph  $G_{\text{adj}}$  with edge costs  $\tilde{\mathcal{C}}_e$  and weights  $\delta_e$

- 1: **for** each edge  $e \in E$  **do**
  - 2:   Identify intersecting obstacles:  $X_e \leftarrow \{x \in X : D(x) \cap e \neq \emptyset\}$
  - 3:   Compute length:  $\ell_e \leftarrow \|v_1(e) - v_2(e)\|$
  - 4:   Compute risk:  $r_e \leftarrow \frac{1}{2} \sum_{x \in X_e} r_x$
  - 5:   Assign cost:  $\tilde{\mathcal{C}}_e \leftarrow \ell_e + r_e$
  - 6:   Assign weight:  $\delta_e \leftarrow \frac{1}{2} \sum_{x \in X_e} \delta_x$
  - 7: **end for**
- 

This preprocessing step equips the graph with risk-aware traversal costs and normalized disambiguation weights, facilitating efficient Lagrangian-based optimization under resource constraints. It bridges the probabilistic obstacle model with deterministic path planning algorithms.

### 3 COLOGR: A Lagrangian & Graph-Reduction Framework

We address the constrained RCDP problem in Equation (3) using a unified framework that combines *Cost- and Obstacle-based Graph Reduction (COGR)* with *Lagrangian Optimization with Graph Reduction (LOGR)*, jointly referred to as the **COLOGR** method.

The COGR phase initiates the process by pruning infeasible or dominated vertices using relaxed versions of the problem that consider cost-only and weight-only criteria. This reduces the size of the graph and tightens optimization bounds before invoking the full solver.

On the reduced graph, the LOGR phase applies a Lagrangian relaxation of the disambiguation constraint by incorporating it into the objective function:

$$\Phi(\lambda) = \min_{p \in \mathcal{P}(s,t)} \left\{ \tilde{\mathcal{C}}_p + \lambda(\delta_p - \delta_{\max}) \right\}, \quad (4)$$

where  $\lambda \geq 0$  is iteratively adjusted to minimize the duality gap. At each iteration, further vertex elimination is performed based on updated feasibility and dominance evaluations relative to the current best bound.

Together, these two phases implement a *Two-Phase Vertex Elimination (TPVE)* strategy that enhances computational efficiency and preserves the optimal solution. The resulting **COLOGR** algorithm integrates structural simplification with dual-guided refinement, producing high-quality paths under resource constraints.

#### 3.1 Path Planning Using Lagrangian Relaxation

For a fixed  $\lambda \geq 0$ , let  $p^\lambda$  denote the  $s$ - $t$  path that minimizes the penalized cost  $\tilde{\mathcal{C}}_p + \lambda\delta_p$ , with corresponding traversal cost  $\tilde{\mathcal{C}}^\lambda$  and disambiguation cost  $\delta^\lambda$ . The function  $\Phi(\lambda) := \tilde{\mathcal{C}}^\lambda + \lambda(\delta^\lambda - \delta_{\max})$  serves as a valid lower bound on the optimal cost, and is maximized to identify a near-optimal Lagrangian multiplier and associated feasible path.

The algorithm begins by evaluating two baseline cases. When  $\lambda = 0$ , the unconstrained minimum-cost path  $p^0$  is computed. If it satisfies  $\delta^0 \leq \delta_{\max}$ , it is optimal and the algorithm terminates. When  $\lambda = \infty$ , the disambiguation term dominates, yielding the minimum-weight path  $p^\infty$ . If  $\delta^\infty > \delta_{\max}$ , no feasible solution exists—this step constitutes the feasibility test. While this situation is avoided in our setting (see Section 5), we retain the test for completeness. Rather than computing  $p^\infty$  via random tie-breaking, we select the shortest obstacle-free path as the minimum-weight solution, improving efficiency.

If neither baseline path resolves the problem, we initialize the upper and lower bounds  $\tilde{\mathcal{C}}_U = \tilde{\mathcal{C}}^\infty$  and  $\tilde{\mathcal{C}}_L = \tilde{\mathcal{C}}^0$ , and proceed with iterative updates over  $\lambda$ .

At each iteration, the algorithm maintains two multipliers,  $\lambda^-$  and  $\lambda^+$ , corresponding to paths  $p^-$  and  $p^+$  such that  $\delta^- < \delta_{\max} < \delta^+$ . A new multiplier  $\lambda_{i+1}$  is computed using the intersection formula (Juttner et al., 2001):

$$\lambda_{i+1} = \frac{\tilde{\mathcal{C}}^- - \tilde{\mathcal{C}}^+}{\delta^+ - \delta^-}. \quad (5)$$

This ensures  $\lambda^+ \leq \lambda_{i+1} \leq \lambda^-$  due to the monotonicity of both cost and disambiguation terms.

The updated path  $p^{\lambda_{i+1}}$  is then computed. Depending on whether its disambiguation cost falls below or above the budget, the pair  $(\lambda^-, p^-)$  or  $(\lambda^+, p^+)$  is updated accordingly. This process continues until the optimal multiplier  $\lambda^*$  is found, as characterized in the following result:

**Proposition 3.1** (Optimality Condition for Lagrange Multiplier). *Let  $p_i^-$  and  $p_i^+$  be the paths with disambiguation costs  $\delta_i^- < \delta_{\max} < \delta_i^+$  and corresponding costs  $\tilde{c}_i^-, \tilde{c}_i^+$ . Let  $\lambda_{i+1}$  be computed via Equation (5), and let  $p_{i+1} := p^{\lambda_{i+1}}$  denote the path minimizing  $\Phi(\lambda)$  at  $\lambda = \lambda_{i+1}$ . Then  $\lambda_{i+1}$  is optimal if either:*

(i)  $\delta_{p_{i+1}} = \delta_{\max};$

(ii) All three paths  $p_i^-, p_i^+$ , and  $p_{i+1}$  attain the same penalized cost at  $\lambda_{i+1}$ :

$$\tilde{c}_{p_{i+1}} + \lambda_{i+1}\delta_{p_{i+1}} = \tilde{c}_i^- + \lambda_{i+1}\delta_i^- = \tilde{c}_i^+ + \lambda_{i+1}\delta_i^+.$$

*Proof.* The dual function  $\Phi(\lambda)$  is concave and piecewise linear, with each path  $p$  contributing a linear segment of slope  $\delta_p - \delta_{\max}$ . If  $p_{i+1}$  satisfies  $\delta_{p_{i+1}} = \delta_{\max}$ , then  $\Phi'(\lambda_{i+1}) = 0$ , and  $\lambda_{i+1}$  is a maximizer. Alternatively, if  $p_i^-, p_i^+$ , and  $p_{i+1}$  yield equal penalized cost at  $\lambda_{i+1}$ , then  $\Phi(\lambda_{i+1})$  lies on the convex hull of the dual function and cannot be improved, ensuring optimality.  $\square$

Despite the method's strength, Lagrangian-based optimization for constrained shortest path problems is not guaranteed to yield an optimal solution in all cases. Two known failure modes include: (i) indistinguishability between multiple paths with equal modified costs, and (ii) exclusion of the true optimal path from those explored by the iterative scheme (Guo and Matta, 2003; Juttner et al., 2001). In our setting, the COGR pruning steps (Section 3.2) reduce such risks by eliminating suboptimal structures early, accelerating convergence and improving solution quality.

### 3.2 Two-Phase Vertex Elimination

To accelerate the Lagrangian optimization process and minimize duality gap risk, we incorporate a graph reduction strategy that eliminates nonessential vertices before and during optimization. Inspired by vertex-pruning heuristics in Muhandiramge and Boland (2009), our approach introduces a two-stage method, termed *Two-Phase Vertex Elimination* (TPVE), that substantially shrinks the graph while preserving the optimal path.

The first phase, **Cost- and Obstacle-based Graph Reduction (COGR)**, operates on structural bounds and applies elimination rules prior to Lagrangian optimization. Since removing a vertex implicitly removes all incident edges, we focus on vertex elimination for greater efficiency. Let  $S_{\min}$  denote any  $(s, t)$ -vertex cut in  $G$ . Then the optimal surrogate cost  $\tilde{c}^*$  is bounded by:

**Property 3.1** (Cut-Based Cost Bounds). *Let  $S_{\min}$  be a minimum  $(s, t)$ -vertex cut. Then*

$$\min_{\substack{p \in \mathcal{P}(s,t) \\ p \cap S_{\min} \neq \emptyset}} \tilde{c}_p^0 \leq \tilde{c}^* \leq \min_{\substack{p \in \mathcal{P}(s,t) \\ \delta_p \leq \delta_{\max}, p \cap S_{\min} \neq \emptyset}} \tilde{c}_p^\infty.$$

The result enables targeted pruning based on vertex-local evaluations of cost and feasibility. Specifically, for each vertex  $v$ , we compute the shortest path through  $v$  using both minimum weight ( $\lambda = \infty$ ) and minimum cost ( $\lambda = 0$ ) criteria, denoted  $p_v^\infty$  and  $p_v^0$ , respectively. If  $p_v^\infty$

violates the disambiguation constraint, then  $v$  cannot lie on any feasible path and is removed. If  $p_v^0$  exceeds the current best upper bound  $\tilde{\mathcal{C}}_U$ , it is also pruned. These checks are applied dynamically during graph scanning, with bounds updated as feasible candidates are encountered. This phase either identifies the optimal solution  $p^*$  or tightens the search interval  $[\tilde{\mathcal{C}}_L, \tilde{\mathcal{C}}_U]$  for subsequent optimization.

To ensure the validity of this reduction process, it is essential to verify that the original  $p^*$  is preserved within the reduced graph (see Corollary 3.1).

The second phase, **Lagrangian Optimization with Graph Reduction (LOGR)**, integrates vertex pruning directly into the Lagrange multiplier update process. At each iteration with multiplier  $\lambda_i$ , we compute for every vertex  $v$  the shortest modified-cost path  $p_v^{\lambda_i}$  and use it to update the upper bound (if feasible) or dual lower bound (if not). A vertex  $v$  is eliminated if its associated dual value at  $\lambda_i$  exceeds the current best upper bound. This pruning continues throughout the optimization cycle, and termination occurs when either the optimal multiplier  $\lambda^*$  is identified (per Proposition 3.1) or the duality gap is closed ( $\tilde{\mathcal{C}}_L = \tilde{\mathcal{C}}_U$ ).

As with COGR, results similar to Proposition 3.2 can be provided to ensure that the optimal path  $p^*$  is not removed from the graph throughout the second phase of vertex elimination.

Our TPVE method differs from earlier SNE strategies (Muhandiramge and Boland, 2009) in three critical aspects: (i) it employs a pre-optimization reduction phase (COGR); (ii) it uses a convergence-aware stopping condition that aligns with Proposition 3.1; and (iii) it retains vertices whose lower bounds match the current upper bound, preserving potential ties in penalized cost and preventing premature elimination of optimal candidates. These enhancements collectively yield significant performance gains and robust convergence guarantees, as justified in Section 3.4 and demonstrated in Section 5.

### 3.3 COLOGR: Combining TPVE & Lagrangian Search

---

#### Algorithm 2 Unified Lagrangian Optimization with Graph Reduction (COLOGR)

---

**Input:** Adjusted graph  $G_{\text{adj}}$  (from Algorithm 1), source  $s$ , target  $t$ , budget  $\delta_{\text{max}}$   
**Output:** Optimal or best feasible path  $p^*$

- 1: Initialize  $V_{\text{del}} \leftarrow \emptyset, E_{\text{del}} \leftarrow \emptyset$
- 2: Compute  $p^\infty$  (min-weight path) and  $p^0$  (min-cost path)
- 3: **if**  $\delta_{p^0} \leq \delta_{\text{max}}$  **then return**  $p^* = p^0$
- 4: **end if**
- 5: Set bounds:  $p_U \leftarrow p^\infty, p_L \leftarrow p^0$
- 6: **repeat** ▷ Phase 1: Vertex Elimination (COGR)
- 7:   **for**  $v \in V(G_{\text{adj}})$  **do**
- 8:     Compute  $p_v^\infty, p_v^0$
- 9:     **if**  $\delta_{p_v^\infty} > \delta_{\text{max}}$  or  $\tilde{C}_{p_v^0} > \tilde{C}_{p_U}$  **then**
- 10:       Eliminate  $v$ :  $V_{\text{del}} \leftarrow V_{\text{del}} \cup \{v\}$ ;
- 11:       Remove incident edges:  $E_{\text{del}} \leftarrow E_{\text{del}} \cup \{e \in E : v \in e\}$
- 12:       Update  $G_{\text{adj}} \leftarrow G(V \setminus V_{\text{del}}, E \setminus E_{\text{del}})$
- 13:     **else if**  $\tilde{C}_{p_v^\infty} < \tilde{C}_{p_U}$  or  $\tilde{C}_{p_v^0} < \tilde{C}_{p_U}$  &  $\delta_{p_v^0} \leq \delta_{\text{max}}$  **then**
- 14:       Update  $p_U \leftarrow p_v^\infty$  or  $p_U \leftarrow p_v^0$
- 15:     **end if**
- 16:   **end for**
- 17: **until** no further eliminations
- 18: **while** duality gap remains open **do**
- 19:    $\lambda \leftarrow \frac{\tilde{C}_{p_U} - \tilde{C}_{p_L}}{\delta_{p_L} - \delta_{p_U}}$
- 20:   Find  $p_\lambda$  minimizing  $\tilde{C}_p + \lambda \delta_p$
- 21:   **if**  $\delta_{p_\lambda} = \delta_{\text{max}}$  **then return**  $p^* = p_\lambda$
- 22:   **end if**
- 23:   **for**  $v \in V(G_{\text{adj}})$  **do** ▷ Phase 2: Vertex Elimination (LOGR)
- 24:     Compute  $p_{\lambda,v}$  through  $v$
- 25:     **if**  $\tilde{C}_{p_{\lambda,v}} < \tilde{C}_{p_U}$  and  $\delta_{p_{\lambda,v}} \leq \delta_{\text{max}}$  **then**
- 26:       Update  $p_U \leftarrow p_{\lambda,v}$
- 27:     **else if**  $\Phi(\lambda, p_{\lambda,v}) > \tilde{C}_{p_U}$  **then**
- 28:       Eliminate  $v$ :  $V_{\text{del}} \leftarrow V_{\text{del}} \cup \{v\}$ ;
- 29:       Remove incident edges:  $E_{\text{del}} \leftarrow E_{\text{del}} \cup \{e \in E : v \in e\}$
- 30:       Update  $G_{\text{adj}} \leftarrow G(V \setminus V_{\text{del}}, E \setminus E_{\text{del}})$
- 31:     **end if**
- 32:   **end for**
- 33:   Update  $p_L$  and bounds
- 34: **end while**
- 35: **return**  $p^* = p_U$

---

**Remark.** Throughout this manuscript, we use the terms *COLOGR* and *Two-Phase Vertex Elimination (TPVE)* interchangeably. They refer to the same unified graph reduction and optimization framework introduced in Sections 3.3–3.2. Specifically, COLOGR is the algorithmic realization of TPVE, combining pre-optimization reduction (COGR) with in-process vertex pruning guided by Lagrangian dual bounds (LOGR). All theoretical results and simulation benchmarks reported under the TPVE name are based on the implementation given in Algorithm 2.  $\square$

### 3.4 Guarantees and Complexity of COLOGR

We now provide guarantees on solution correctness and computational complexity. These results justify the effectiveness of TPVE when integrated with the Lagrangian scheme, establishing that no part of the true optimal path is pruned despite aggressive graph reduction. The following proposition ensures that the constrained optimal solution is preserved through both phases of TPVE.

**Proposition 3.2** (Preservation of Optimal Path under TPVE). *Let  $p^*$  be the optimal solution to the RCDP problem with total approximate cost  $\tilde{\mathcal{C}}^*$  and disambiguation cost  $\delta_{p^*} \leq \delta_{\max}$ . Then the path  $p^*$  is retained in the graph after both COGR and LOGR phases of TPVE.*

*Proof.* Let  $p^*$  be an optimal  $s$ - $t$  path such that  $\delta_{p^*} \leq \delta_{\max}$  and  $\tilde{\mathcal{C}}_{p^*} = \tilde{\mathcal{C}}^*$ . Consider any vertex  $v \in p^*$ .

In Phase 1 (COGR),  $v$  is preserved if: (i) there exists a feasible path through  $v$  with  $\delta_p \leq \delta_{\max}$ , and (ii) at least one such path has cost no greater than the current upper bound  $\tilde{\mathcal{C}}_U$ . Both conditions hold for  $p^*$ , so  $v$  is not eliminated.

In Phase 2 (LOGR),  $v$  is preserved if the lower bound of the optimal path cost via  $v$  does not exceed the current upper bound, i.e.,  $\Phi(\lambda, p_{\lambda,v}) \leq \tilde{\mathcal{C}}_{p_U}$ . For  $v$  that lies on  $p^*$ , any identified lower bound  $\Phi(\lambda, p_{\lambda,v})$  always satisfies  $\Phi(\lambda, p_{\lambda,v}) \leq \tilde{\mathcal{C}}_{p^*}$ , and the current upper bound satisfies  $\tilde{\mathcal{C}}_U \geq \tilde{\mathcal{C}}_{p^*}$ , since no feasible path can be cheaper than the optimal one. Therefore,  $v$  is not eliminated.

Since this reasoning applies to every vertex  $v \in p^*$  and both phases of TPVE, the entire path  $p^*$  remains in the final reduced graph.  $\square$

The following corollary isolates the preservation guarantee under Phase 1 of TPVE. It formalizes the intuitive observation that the optimal path  $p^*$  remains in the graph as long as it is both feasible and cost-competitive under initial pruning rules.

**Corollary 3.1** (Preservation under Phase 1 Only). *Under the same assumptions as Proposition 3.2, the optimal path  $p^*$  is preserved after Phase 1 of TPVE.*

As noted earlier in Section 3.1, the Lagrangian relaxation method may fail to recover the optimal path in certain degenerate cases. Nevertheless, in all simulation replications reported in Section 5, our proposed algorithm (COLOGR) consistently produced the optimal solution  $p^*$ . This section offers a structural explanation for this empirical robustness, focusing on cases with non-unique minimizers of the Lagrangian objective.

One such scenario involves multiple paths minimizing the modified cost  $\tilde{\mathcal{C}}_p + \lambda\delta_p$ , only one of which corresponds to the true optimal path  $p^*$  with respect to the original cost  $\tilde{\mathcal{C}}$ . While the standard Lagrangian framework does not guarantee recovery of  $p^*$  in this setting, the integration of the two-phase graph reduction process (TPVE) can resolve the ambiguity. The following proposition formalizes a sufficient condition for successful identification of  $p^*$  in this case.

**Proposition 3.3** (Identification of  $p^*$  via Unique Vertex Signature). *Suppose that for some Lagrange multiplier  $\lambda^*$ , multiple  $(s, t)$ -paths minimize the Lagrangian cost*

$$\tilde{\mathcal{C}}_p + \lambda^*(\delta_p - \delta_{\max}),$$

and that the true optimal path  $p^*$  for the RCDP problem is among them. If there exists a vertex  $v \in p^*$  such that no other minimum-cost path (at  $\lambda^*$ ) passes through  $v$ , then the TPVE algorithm correctly identifies  $p^*$ .

*Proof.* Since  $p^*$  is feasible and attains the minimum relaxed cost at  $\lambda^*$ , it satisfies both the constraint  $\delta_{p^*} \leq \delta_{\max}$  and the dual optimality condition. By assumption, vertex  $v \in p^*$  is exclusive to  $p^*$  among all minimum-cost paths at  $\lambda^*$ . The COLOGR algorithm (implementing the TPVE framework) evaluates, for each vertex, the best path passing through it. For  $v$ , this path must be  $p^*$ , as no other minimum-cost path shares that vertex. Thus, the vertex-specific structure uniquely identifies  $p^*$ , allowing the algorithm to recover it even in the presence of ties.  $\square$

The previous result demonstrates how structural uniqueness—via exclusive vertex participation—can resolve ambiguity among multiple dual minimizers and guide the TPVE subroutine to the correct path.

Beyond this, the COLOGR algorithm often succeeds even in the absence of structural uniqueness or zero duality gap. In particular, when the optimal path  $p^*$  is feasible and minimizes the Lagrangian cost for some multiplier  $\lambda \geq 0$ , our algorithm still identifies  $p^*$  correctly. This robustness explains the consistent empirical performance observed in Section 5, even under conditions where strong duality is not theoretically guaranteed.

**Proposition 3.4** (Correct Recovery under Dual Attainment). *Suppose the optimal path  $p^*$  for the RCDP problem is feasible, i.e.,  $\delta_{p^*} \leq \delta_{\max}$ , and also minimizes the Lagrangian objective for some  $\lambda \geq 0$ :*

$$p^* \in \arg \min_{p \in \mathcal{P}(s,t)} \left\{ \tilde{\mathcal{C}}_p + \lambda(\delta_p - \delta_{\max}) \right\}.$$

*Then the COLOGR algorithm correctly identifies  $p^*$  as the optimal path, and  $\lambda$  serves as an optimal Lagrange multiplier.*

*Proof.* Assume  $p^*$  is feasible and minimizes the relaxed cost function at  $\lambda$ , i.e.,

$$\tilde{\mathcal{C}}_{p^*} + \lambda(\delta_{p^*} - \delta_{\max}) = \Phi(\lambda),$$

where  $\Phi(\lambda)$  is the Lagrangian dual function. We consider two cases:

**Case 1:**  $\delta_{p^*} = \delta_{\max}$ . Then the penalty term vanishes, and  $\Phi(\lambda) = \tilde{\mathcal{C}}_{p^*}$ . Since  $p^*$  is feasible and attains this minimum, strong duality holds, and COLOGR terminates with  $p^*$  as the optimal path.

**Case 2:**  $\delta_{p^*} < \delta_{\max}$ . Although the penalty term becomes negative,  $p^*$  still minimizes the Lagrangian objective at  $\lambda$ . Because  $p^*$  is feasible, its cost updates the best known upper bound  $\tilde{\mathcal{C}}_U$ . Since no subsequent path can improve upon this bound, the upper bound stabilizes at  $\tilde{\mathcal{C}}_{p^*}$ , and COLOGR eventually terminates with  $p^*$ . Moreover, as COLOGR evaluates minimum-cost paths through all vertices in Phase 2, and  $p^*$  is among these, it is guaranteed to be retained.

Thus, regardless of whether the constraint is active at optimality, the COLOGR algorithm recovers  $p^*$  and identifies the corresponding  $\lambda$  as optimal.  $\square$

Building on Proposition 3.4, we now examine a complementary setting in which the optimal RCDP path  $p^*$  satisfies  $\delta_{p^*} = \delta_{\max}$  but is not among the minimizers of the Lagrangian objective

at the corresponding dual optimum. Suppose under the optimal multiplier  $\lambda^*$ , there exist two paths  $p_1$  and  $p_2$  satisfying:

$$\tilde{C}_{p_1} + \lambda^*(\delta_{p_1} - \delta_{\max}) = \tilde{C}_{p_2} + \lambda^*(\delta_{p_2} - \delta_{\max}) < \tilde{C}^*, \quad (6)$$

with  $\delta_{p_1} > \delta_{\max}$  and  $\delta_{p_2} < \delta_{\max}$ . Although  $p_1$  violates the disambiguation budget and  $p_2$  underutilizes it, neither satisfies the constraint with equality as  $p^*$  does; hence,  $p^*$  is excluded from the argmin of the dual objective at  $\lambda^*$ , despite being optimal under the original constraint. The propositions below show that despite this, the proposed TPVE algorithm correctly identifies  $p^*$  in both special and general cases.

**Remark 3.1. (Assumptions for Propositions 3.5–3.7)** We first state some assumptions and introduce notation to be used in Propositions 3.5–3.7 below. Let  $X = \{x_1, \dots, x_k\}$  be a finite set of  $k \geq 2$  ambiguous obstacles, each with disambiguation cost  $\delta_x > 0$ . Let  $\delta_{\max} > 0$  be the total disambiguation budget, and let  $B$  be the maximal number of disambiguations permitted under this budget; i.e., at most  $B$  obstacles  $x$  can be disambiguated such that  $\sum_{x \in S} \delta_x \leq \delta_{\max}$  for all  $S \subseteq X$  with  $|S| \leq B$ . Suppose there exists a path  $p^*$  that intersects a subset of obstacles  $X^* \subseteq X$  such that: (i)  $|X^*| \leq B$ , and  $\sum_{x \in X^*} \delta_x \leq \delta_{\max}$ ; (ii) any other path  $p \neq p^*$  either intersects a set  $X_p$  of obstacles with  $\sum_{x \in X_p} \delta_x > \delta_{\max}$  (infeasible), or avoids all obstacles but incurs strictly higher cost than  $p^*$ .

**Proposition 3.5** (Correct Identification in a Two-Obstacle Scenario). *In an RCDP instance under the assumptions in Remark 3.1 with  $k = 2$  and  $|X^*| = B = 1$  (i.e. supposing there are  $k = 2$  ambiguous obstacles  $X = \{x_1, x_2\}$  in the environment, with  $\min\{\delta_{x_1}, \delta_{x_2}\} \leq \delta_{\max} < \max\{\delta_{x_1}, \delta_{x_2}\}$  and  $p^*$  intersects exactly one of the obstacles, while any other path  $p \neq p^*$  intersects both (infeasible) or neither but more costly than  $p^*$ ) the COLOGR algorithm correctly eliminates non-optimal paths and identifies  $p^*$  as optimal.*

**Proposition 3.6** (Identification under Single Disambiguation Budget). *In an RCDP instance under the assumptions in Remark 3.1 with  $k \geq 2$  and  $|X^*| = B = 1$  (i.e. supposing there are  $k \geq 2$  ambiguous obstacles  $X = \{x_1, \dots, x_k\}$ , and the disambiguation budget satisfies  $\delta_{\max} < \min_{x_i+x_j} \delta_{x_i} + \delta_{x_j}$  for all distinct  $x_i, x_j \in X$ , and that there exists a feasible path  $p^*$  intersecting exactly one obstacle  $x^*$  such that  $\delta_{x^*} \leq \delta_{\max}$ ) and all other paths satisfy condition (ii) of Remark 3.1. COLOGR algorithm eliminates all such non-optimal paths and identifies  $p^*$  as the optimal path.*

**Proposition 3.7** (Identification under  $B$ -Budget Disambiguation). *Under the assumptions of Remark 3.1 with general  $k \geq 2$ ,  $B \geq 1$  and  $|X^*| \leq B$  COLOGR algorithm eliminates all such non-optimal paths and identifies  $p^*$  as the optimal path.*

**Remark 3.2.** Note that in practice, we assume  $B \leq k$ , since at most  $k$  distinct obstacles can be disambiguated. If  $B > k$ , then  $B$  becomes redundant, and the only active constraint is whether the total disambiguation cost  $\sum_{x \in S} \delta_x$  for any  $S \subseteq X$  satisfies  $\sum_{x \in S} \delta_x \leq \delta_{\max}$ .

The results in Propositions 3.5–3.7 (proof provided in the Appendix (Section A2.2)) establish that even when the Lagrangian objective does not favor the optimal path  $p^*$ , the structural pruning performed by TPVE preserves and ultimately identifies it. This includes scenarios where dual-optimal paths  $p_1$  and  $p_2$  mislead the optimizer despite being infeasible or suboptimal, as formalized in Equation (6).

To further illustrate the utility of structural pruning, consider the representative case from Proposition 3.5, where three competing paths exist:  $p_1$  (infeasible with lower cost),  $p_2$  (obstacle-free but costly), and  $p^*$  (feasible and optimal under the constraint). Although  $p_1$  violates the disambiguation budget ( $\delta_{p_1} > \delta^*$ ) and  $p_2$  is feasible but longer ( $\delta_{p_2} < \delta^*$ ,  $\tilde{C}_{p_2} > \tilde{C}^*$ ), the penalty structure in the dual formulation can cause both to appear superior to  $p^*$  under certain multipliers, as illustrated in Equation (6).

To mitigate this distortion and improve alignment between the dual and primal solutions, we adopt a strategy that increases the relative influence of the true traversal cost  $\tilde{C}_p$  over the penalty term  $\lambda(\delta_p - \delta_{\max})$ . This is achieved by tuning the risk function parameters so that the risk term  $r_p$  more sharply reflects obstacle uncertainty. In the RCDP setting,  $r_p$  is determined by the structure of the environment and a user-defined exploration parameter (e.g.,  $\alpha$  in the linear undesirability model), along with the blockage probability marks  $\pi_X$ .

While disambiguation costs and obstacle probabilities are externally specified, the planner can still regulate the sensitivity of risk through the choice of risk function and its parameters. To formalize this idea, we define the *risk blockage gradient (RBG)* as a measure of how steeply the path risk  $r_p$  increases with blockage probability. This formulation generalizes the role of tuning parameters like  $\alpha$  in the LU model by framing sensitivity in terms of a gradient concept applicable across risk models.

A higher RBG imposes steeper penalties on ambiguous paths, improving the separation between feasible and infeasible solutions in the dual objective. This enhances the convergence of COLOGR and reduces the likelihood of spurious dual optima.

Similar arguments apply when  $\delta^* < \delta_{\max}$ , though this case is often ruled out by structural dominance. If a feasible path with  $\delta_p = \delta_{\max}$  has higher cost than  $p^*$ , and  $p^*$  requires less disambiguation, then  $p^*$  dominates such paths in both feasibility and cost. Realistically, adversarial environments are designed to avoid such dominance relationships, further supporting the utility of dual-guided reduction.

This intuition is formalized in the following property (proof provided in the Appendix (Section A2.3)).

**Property 3.2** (Spurious Dual Optima Vanish under High RBG). *Let  $p^*$  denote the optimal path for the RCDP problem, and let  $\lambda^*$  be a Lagrange multiplier such that multiple paths minimize the relaxed objective  $\tilde{C}_p + \lambda^*(\delta_p - \delta_{\max})$ . Suppose some of these minimizers are either infeasible or sub-optimal under the original constraint. Then, as the risk blockage gradient (RBG) increases—i.e., as the risk function becomes more sensitive to blockage probabilities—the likelihood that such spurious paths remain dual-optimal diminishes. For sufficiently high RBG, the surrogate cost  $\tilde{C}_p$  dominates the dual objective, aligning the relaxed minimizers with the true constrained optimum  $p^*$ .*

We next analyze the worst-case time complexity of the proposed COLOGR algorithm.

**Theorem 3.1** (Time Complexity of COLOGR Algorithm). *Let  $G = (V, E)$  be a spatial grid graph with  $n_v = |V|$  vertices and  $n_e = |E|$  edges. Then the COLOGR algorithm solves the RCDP problem with worst-case time complexity:*

$$\mathcal{O}(n_v n_e^2 \log n_e (n_e + n_v \log n_v)).$$

*Proof.* The COLOGR algorithm proceeds in two phases:

In **Phase 1**, COGR applies vertex pruning based on feasibility and cost bounds. Each iteration involves:

1. Computing shortest paths with respect to weight and cost via Dijkstra’s algorithm:  $\mathcal{O}(n_e + n_v \log n_v)$ .
2. Evaluating elimination criteria and updating bounds:  $\mathcal{O}(n_v + n_e)$ .

This phase may iterate over all  $n_v$  vertices, leading to a total cost of  $\mathcal{O}(n_v(n_e + n_v \log n_v))$ .

In **Phase 2**, LOGR solves the Lagrangian relaxation using breakpoint updates over the multiplier  $\lambda$ . The number of breakpoints is bounded by  $\mathcal{O}(n_e^2 \log n_e)$  (Jüttner, 2005), and each iteration involves a shortest path computation and vertex-level updates, costing  $\mathcal{O}(n_v(n_e + n_v \log n_v))$ . Hence, the total cost of LOGR is:

$$\mathcal{O}(n_v n_e^2 \log n_e (n_e + n_v \log n_v)).$$

The overall complexity is dominated by Phase 2, establishing the stated bound.  $\square$

In practice, the initial pruning in COGR substantially reduces the graph size, leading to faster convergence in the Lagrangian phase. This yields a notable improvement over baseline methods such as SNE, which incur higher complexity of  $\mathcal{O}(n_v^2 n_e^2 \log^4 n_e (n_e + n_v \log n_v))$ .

## 4 Design and Analysis of the RCDP Traversal Policy

Building on the COLOGR algorithm introduced in Section 3.3, we now present the complete *RCDP traversal protocol*, which integrates duality-based optimization with two-phase graph reduction. This section formalizes the traversal strategy, establishes theoretical guarantees, and illustrates its behavior using a stylized grid-based example. The decision process is visualized in Figure 1, and appendix provides detailed path visualizations and execution logs for reproducibility.

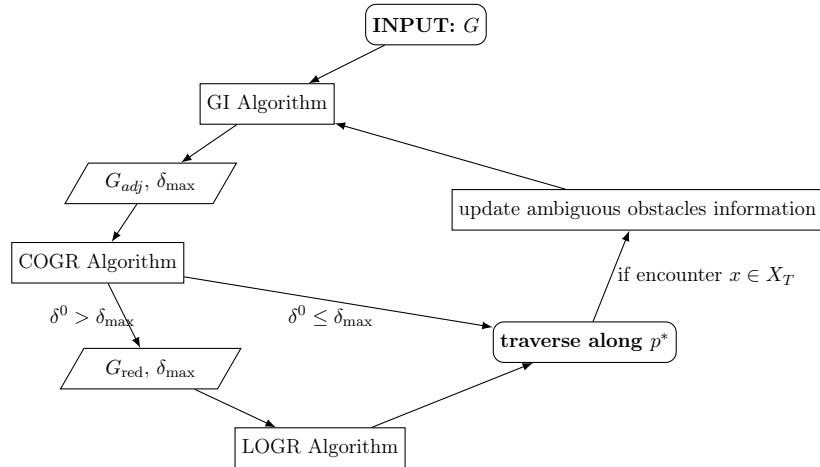


Figure 1: Schematic overview of the RCDP traversal protocol (Algorithm 3).

## 4.1 Algorithmic Framework

The RCDP policy operates on the adjusted graph  $G_{\text{adj}}$  generated by Algorithm 1. At each step, it solves the constrained surrogate optimization problem in Equation (3), examines the first edge of the resulting path, and decides whether to disambiguate based on the available budget. If disambiguation is feasible, the agent updates obstacle information; otherwise, it re-plans accordingly.

The full traversal logic is provided in Algorithm 3. The subroutines comprising COLOGR are detailed in the Appendix.

---

### Algorithm 3 RCDP Traversal Policy

---

**Input:**  $G_{\text{adj}}$ , start  $s$ , target  $t$ ; risk function  $r_x$ ; disambiguation budget  $\delta_{\text{max}}$   
**Output:** Traversal path  $p^*$

- 1:  $v \leftarrow s$ ;  $p \leftarrow \{s\}$
- 2: **while**  $v \neq t$  **do**
- 3:     Compute path  $p^{\text{next}}$  from  $v$  to  $t$  via Equation (3)
- 4:     Let  $e = (v, u)$  be the first edge on  $p^{\text{next}}$
- 5:     **if**  $e$  intersects ambiguous obstacle  $x$  **then**
- 6:         Disambiguate  $x$ ;  $\delta_{\text{max}} \leftarrow \delta_{\text{max}} - \delta_x$
- 7:         **if**  $x$  is blocking **then continue** ▷ Re-plan due to blocked edge
- 8:         **end if**
- 9:     **end if**
- 10:     $v \leftarrow u$ ;  $p \leftarrow p \cup \{u\}$
- 11: **end while**
- 12: **return**  $p^* = p$

---

## 4.2 Theoretical Guarantees and Benchmark Comparison

In this section, we establish key theoretical guarantees for the proposed RCDP policy. We focus on two aspects: (i) feasibility with respect to the disambiguation budget constraint, and (ii) optimality of the surrogate cost under the selected risk function. We then compare the performance of RCDP and greedy traversal policies under a unified risk modeling framework.

**(i) Feasibility:** Let  $\delta_p$  denote the total disambiguation cost incurred along path  $p$ . By construction, Algorithm 3 ensures that the disambiguation budget constraint  $\delta_p \leq \delta_{\text{max}}$  is respected throughout the traversal. This guarantees that the disambiguation budget constraint is never violated throughout the traversal.

**(ii) Approximate Optimality in Surrogate Metric:** At each iteration, the solver for the Lagrangian-relaxed problem in Equation (3) returns a globally optimal path on the reduced graph, minimizing the surrogate cost  $\tilde{\mathcal{C}}_p$  over the current feasible set. The graph reduction procedure, executed via COLOGR Algorithm, preserves  $s$ - $t$  connectivity and ensures that surrogate cost comparisons among retained paths remain valid, thereby supporting consistent surrogate optimization after graph reduction.

**Theorem 4.1** (Feasibility and Surrogate Optimality of COLOGR). *Let  $G_{\text{adj}} = (V, E)$  be the reduced graph produced by the COLOGR algorithm for the RCDP problem, and let  $r_x$  be a fixed risk function used to compute the surrogate edge cost  $r_e$  for each edge  $e \in E$ . Let  $\tilde{\mathcal{C}}_p = \sum_{e \in p} (\ell_e + r_e)$  denote the surrogate cost for path  $p \in \mathcal{P}(s, t; G_{\text{adj}})$ , as introduced in Equation (2). Assume that there exists a path  $p^* \in \mathcal{P}(s, t; G_{\text{adj}})$  that both minimizes the Lagrangian-relaxed objective at*

the optimal multiplier  $\lambda^*$  and satisfies the budget constraint  $\delta_{p^*} \leq \delta_{\max}$ . Then  $p^*$  is a feasible surrogate-optimal solution:

$$\delta_{p^*} \leq \delta_{\max}, \quad \text{and} \quad \tilde{\mathcal{C}}_{p^*} = \min \left\{ \tilde{\mathcal{C}}_p : p \in \mathcal{P}(s, t; G_{adj}), \delta_p \leq \delta_{\max} \right\}.$$

*Proof provided in the Appendix (Section A2.4).*

**Comparison with Greedy Policies.** In low-density environments or when the disambiguation budget is relatively high (e.g.,  $n = 20$  or  $40$  obstacles, and maximum number of disambiguation allowed is  $N_{\max} = 3$  or a total cost limit  $\delta_{\max} = 4, 6$ ), some greedy policies may appear competitive with RCDP variants. This is expected, as the advantage of informed disambiguation is less pronounced in such scenarios. Nonetheless, across a wide range of settings and under consistent risk modeling, the RCDP policy demonstrably yields lower expected traversal costs than its greedy counterparts.

We now formalize this performance guarantee under the assumption that the risk function  $r_x$  used to define  $\tilde{\mathcal{C}}_p$  is nondecreasing in the disambiguation cost  $\delta_x$  and nondecreasing in the probability of blockage ( $\pi_x$ ).

**Property 4.1. (Conditional Dominance of RCDP Policy)** *Under suitable conditions on the surrogate risk model—specifically, when the risk function is non-decreasing in the probability of obstacle blockage, and surrogate cost ordering is consistent with expected cost ordering—the RCDP policy achieves lower expected traversal cost than any greedy baseline policy that ignores resource constraints in its initial plan.*

*Formal Statement and Proof.* The full proposition and its proof are presented in the Appendix (Section A2.4). This property provides a theoretical justification for the empirical performance advantage of the RCDP policy observed in our experiments (Section 5). While the result relies on strong assumptions regarding surrogate model fidelity, it illustrates how constraint-aware optimization can outperform greedy heuristics, especially in environments with heterogeneous risk and cost structures.

## Bayesian Tuning of Linear Undesirability Risk Function and Consistency Result

To operationalize the linear undesirability (LU) risk function, we examined the impact of the tuning parameter  $\alpha$  on traversal performance across varying obstacle densities and true obstacle proportions. Our results indicate that higher  $\alpha$  values are beneficial in environments with denser true obstacles, as they enhance the policy’s ability to penalize risky paths. We also propose a Bayesian-adjusted extension in which  $\alpha$  is obstacle-specific, determined via posterior estimates of being a true obstacle. Full details, including simulation results and a principled derivation of the Bayesian linear undesirability function  $r^{LB}$ , are provided in the Appendix (Section A3).

Moreover, we show that the RCDP policy using the Bayesian LU risk function achieves asymptotic optimality: as sensor accuracy improves, its expected cost converges to that of the offline benchmark. This convergence result provides further justification for using the Bayesian-adjusted LU model in high-precision settings.

### 4.3 Illustrative Example

To illustrate the RCDP traversal policy and benchmark its performance against a greedy baseline, we consider a simple test case. Specifically, we compare it against the constrained RD policy from Aksakalli and Ari (2014). Extensive simulation-based comparisons are deferred to Section 5.

We define a compact traversal region  $\Omega = [0, 22] \times [0, 14]$  and discretize it using an 8-adjacency integer grid. The source and target locations are  $s = (11, 14)$  and  $t = (11, 1)$ , respectively. Six disk-shaped obstacles of radius  $r = 2.5$  are placed in the region, with blockage probabilities  $\pi = (0.7, 0.2, 0.1, 0.3, 0.1, 0.4)$  and disambiguation costs  $\delta = (1, 2, 1, 1, 2, 2)$ . The traversal budget is  $\delta_{\max} = 2$ .

Figure 2 presents this scenario and the resulting traversals. The RCDP policy—solved using COLOGR with the undesirability risk function ( $\alpha = 15$ )—identifies the optimal path on a reduced graph (panel b). The first disambiguation occurs at obstacle 4. Depending on its status:

- (i) If false, the agent proceeds directly to  $t$  (panel c).
- (ii) If true, a replan is triggered from the disambiguation node with updated budget  $\delta_{\max} = 1$  (panel d).

This results in an expected cost of:

$$\mathbf{E}[\mathcal{C}_p] = 0.7 \cdot (19.8995 + 1) + 0.3 \cdot (23.5563 + 1) = 21.9966.$$

By contrast, the constrained RD policy (panel e) initiates disambiguation at obstacle 3. If it is false, the agent attempts obstacle 5, but its cost exceeds the remaining budget. It then redirects to obstacle 4. If obstacle 3 is true, the agent bypasses directly to obstacle 4. The expected cost is:

$$\begin{aligned} \mathbf{E}[\mathcal{C}_p] &= (0.9 \cdot 0.7)(24.7280 + 2) + (0.1 \cdot 0.7)(20.4853 + 2) \\ &\quad + (0.1 \cdot 0.3)(24.1421 + 2) + (0.9 \cdot 0.3)(31.3136 + 2) = 28.1916, \end{aligned}$$

which is substantially higher than under the RCDP policy.

This example highlights the key advantage of constraint-aware planning: the RCDP policy integrates the disambiguation budget directly into traversal decisions, yielding more cost-effective plans than greedy approaches that lack global constraint awareness.

## 5 Empirical Evaluation via Monte Carlo Simulation

We evaluate the performance of the proposed RCDP policy across a variety of sensor conditions, obstacle densities, and disambiguation budgets using a Monte Carlo simulation framework. The experimental setup is designed to align with a real-world dataset known as COBRA, a minefield navigation dataset frequently used in the literature for testing traversal strategies (Priebe et al. (2005), Ye and Priebe (2010), Aksakalli et al. (2011), Aksakalli et al. (2016)). We use a rectangular traversal region  $\Omega = [0, 100] \times [0, 50]$ , with start and target points fixed at  $s = (50, 50)$  and  $t = (50, 1)$ , respectively. Obstacles are modeled as disks with centers placed in  $[10, 90] \times [10, 40]$ , promoting route selection through cluttered regions rather than entirely avoiding obstacles.

To maintain clarity, we present illustrative outcomes in the main paper and relegate detailed replication results, extended settings, and sensitivity analyses to the Appendix.

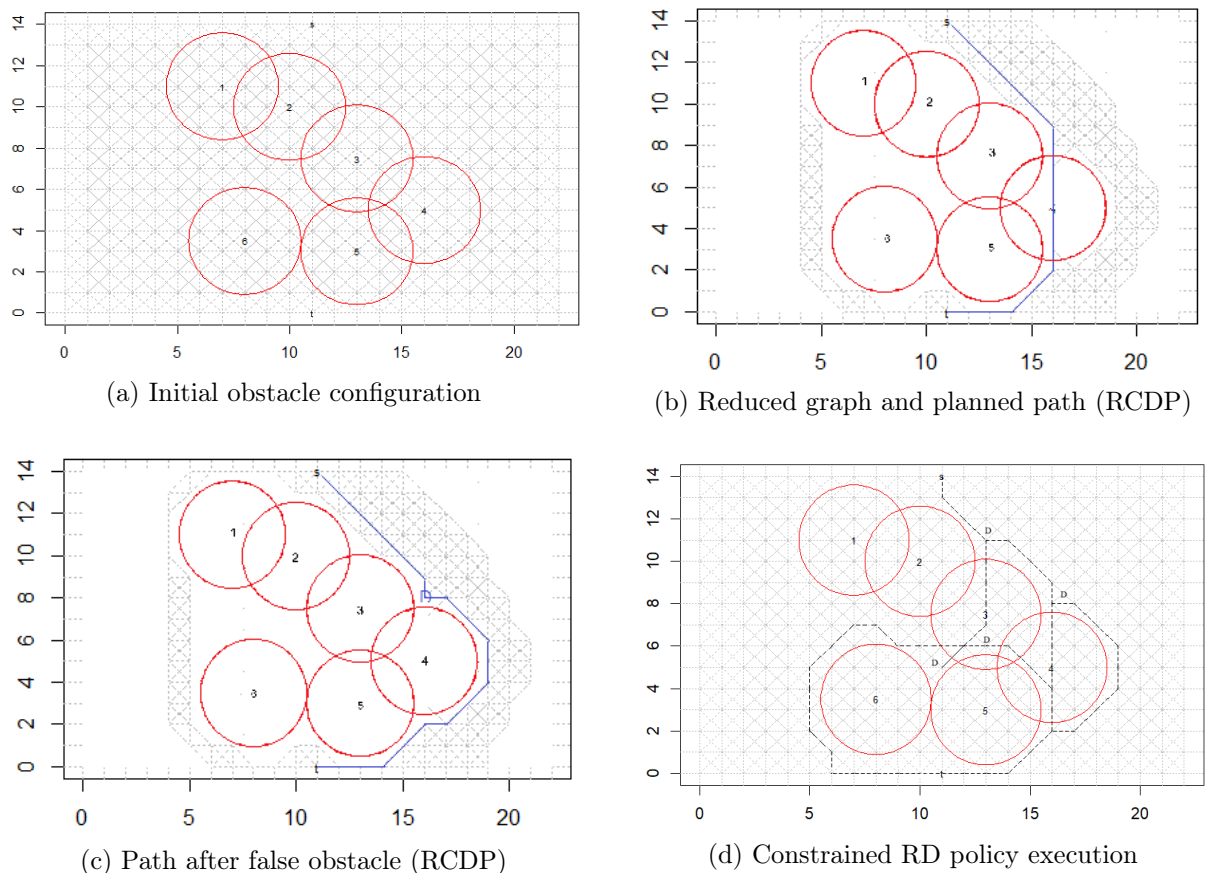


Figure 2: Toy example comparing RCDP with constrained RD policy. Panels (a)–(c) show the RCDP setup and execution under  $\delta_{\max} = 2$ . Panel (d) shows the less efficient behavior of the constrained RD policy.

## 5.1 Simulation Design and Experimental Setup

We simulate traversal scenarios within a rectangular region  $\Omega = [0, 100] \times [0, 50]$  using a discretized 8-adjacency grid. The start and target locations are fixed at  $s = (50, 50)$  and  $t = (50, 1)$ , respectively. Obstacle centers are placed within the subregion  $[10, 90] \times [10, 40]$  to ensure adequate coverage while allowing traversable paths.

**Obstacle Configuration.** We consider three density levels by varying the total number of ambiguous obstacles  $n \in \{20, 40, 80\}$ , with corresponding numbers of true obstacles set as  $n_T = \{4, 8, 16\}$  (i.e., 20% of the obstacles are true). Obstacles are circular with fixed radius 5 and their spatial layout follows a Strauss process with inhibition distance 7 and interaction parameter  $\gamma = 0.5$  to model realistic clustering and mild repulsion (Baddeley, 2010).

**Sensor Precision.** Sensor-reported blockage probabilities  $\pi_x$  follow a two-component beta model:

$$\pi_x \sim \begin{cases} \text{Beta}(6, 2), & \text{if } x \text{ is a true (blocking) obstacle,} \\ \text{Beta}(2, 6), & \text{if } x \text{ is a false (non-blocking) obstacle.} \end{cases}$$

These asymmetric distributions model a sensor providing higher probabilities for true obstacles and lower probabilities for false obstacles.

**Disambiguation Budget.** Two scenarios are examined:

- (i) *Simplified scenario:* All obstacles require equal cost  $\delta_x = 5$ ; the constraint is interpreted as a hard cap on the number of disambiguations  $N_{\max} \in \{1, 2, 3\}$ .
- (ii) *General scenario:* Each obstacle has an individual cost  $\delta_x \in \{2, 3, 4, 5, 6\}$ , depending on whether it is a true obstacle and its isolation; the total budget is enforced via total cost constraints  $\delta_{\max} \in \{4, 6, 8, 10\}$ .

**Policies and Risk Functions.** We evaluate seven policies:

*Greedy baselines:* constrained RD and constrained DT policies,

*Proposed RCDP variants:* employing the reset risk function, the DT risk function, and the linear undesirability function with  $\alpha \in \{\delta_x, 15, 30\}$ .

For each trial, we record total traversal cost  $\mathcal{C}_p$ , number of disambiguations used, gap from offline-optimal benchmark (i.e., full-information shortest path), constraint satisfaction rate (proportion of paths with  $\delta_p \leq \delta_{\max}$ ).

Table 1: Simulation setting parameters.

$n$	$n_T$	$N_{\max}$	$\delta_{\max}$
20	4	1, 2, 3	4, 6
40	8	1, 2, 3	6, 8
80	16	1, 2, 3	8, 10

## 5.2 Performance Comparison

Figure 3 shows the average traversal cost and standard deviation of each risk-based policy across environments: different obstacle density levels, neutral sensor marks, and varying budget levels.

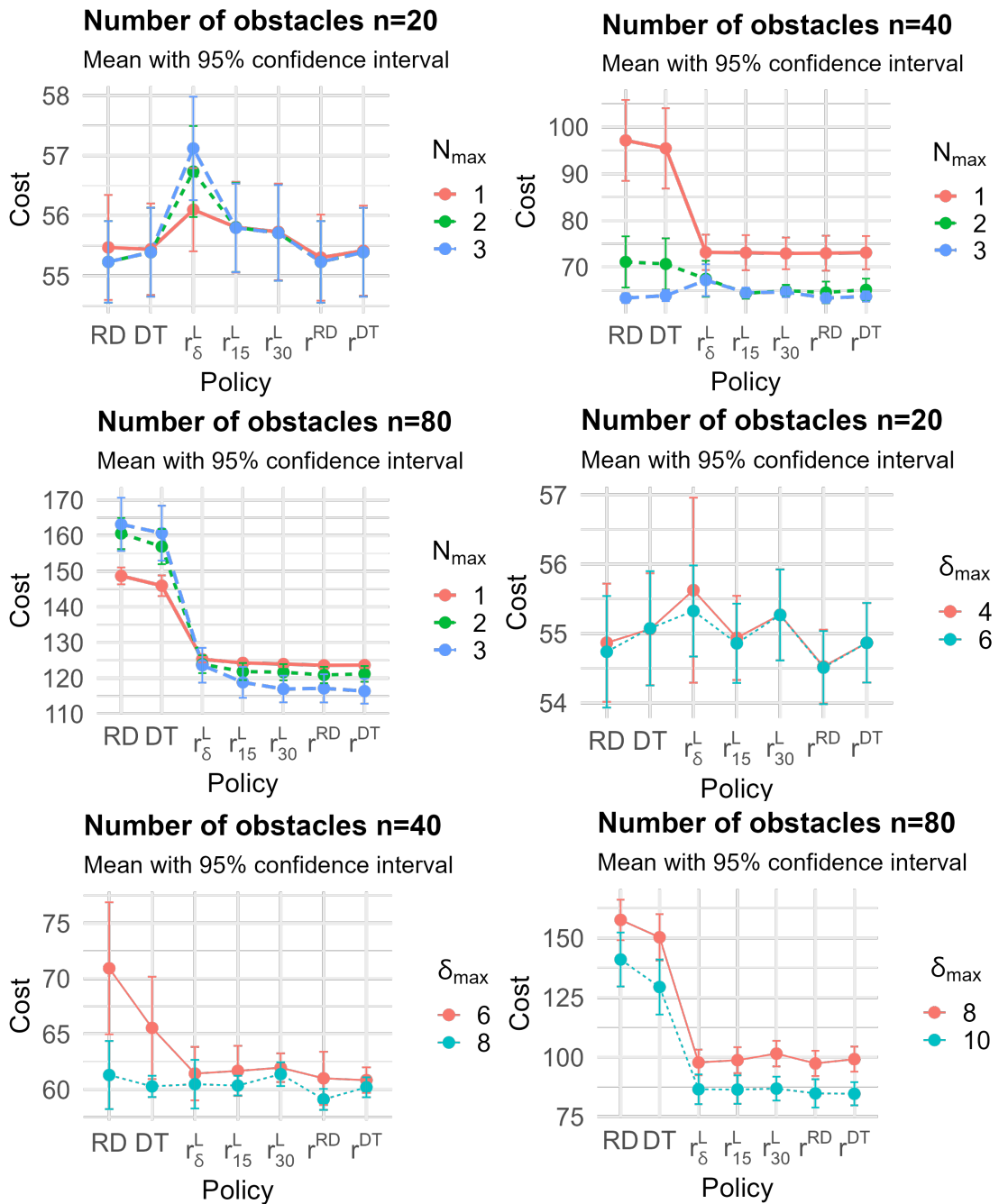


Figure 3: The average traversal cost with 95% confidence interval of two greedy policies, five RCDP policies with different risk functions

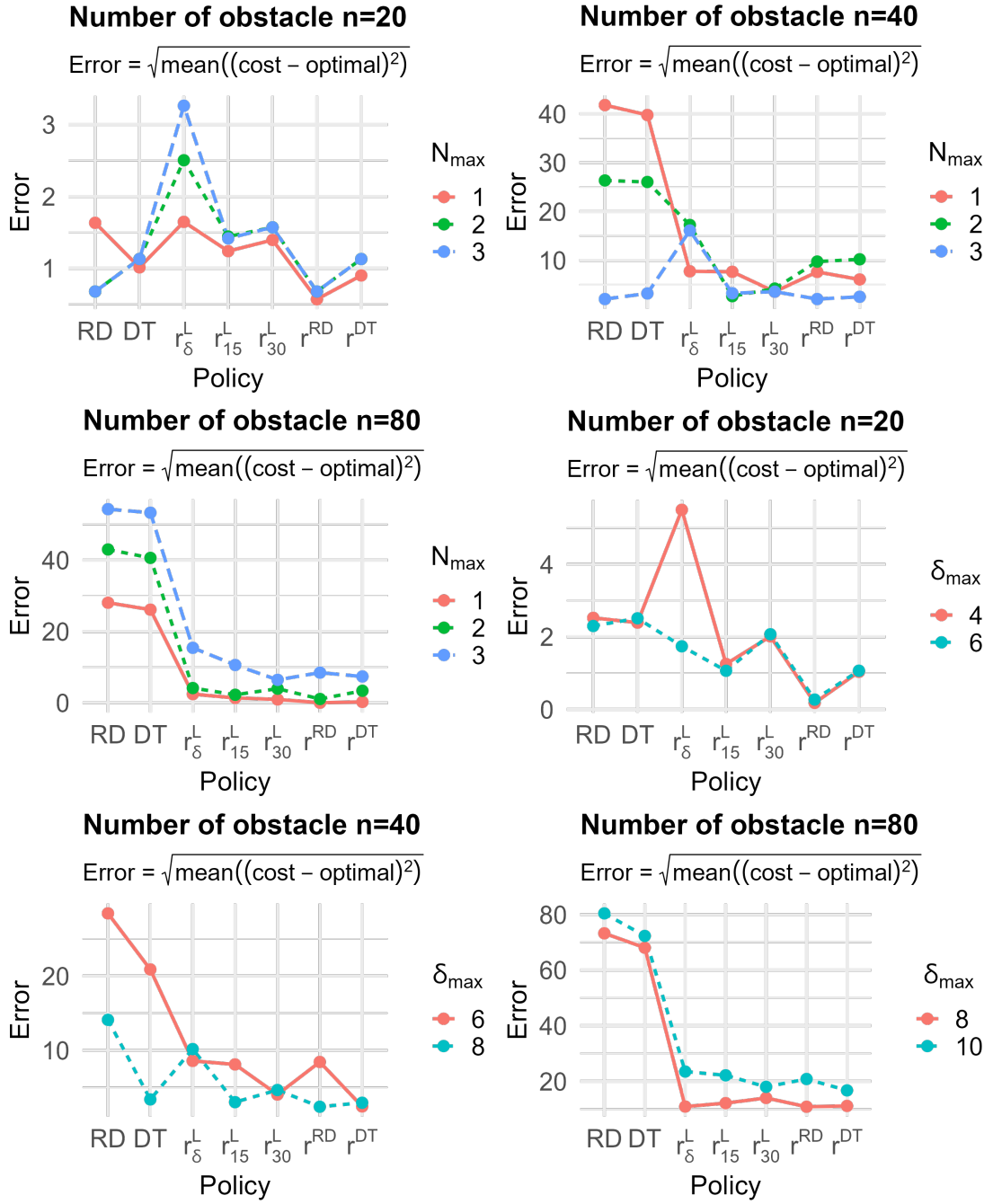


Figure 4: The deviation of two greedy policies, five RCDP policies with different risk functions from optimal solutions

Beyond average cost, we assess each policy's proximity to the offline-optimal benchmark. Figure 4 illustrates the deviation from optimal across environments, confirming that RCDP policies maintain closer adherence to ideal paths, especially under dense obstacles and tight budgets.

	Greedy Policies		WCSPP Policies		
	RD	DT	$r^{RD}$	$r^{DT}$	$r_{\alpha^*}^L$
$N_{\max} = 1$	149.50	149.50	125.53	125.53	<b>122.91</b>
	151.25	151.25	117.25	121.43	<b>117.25</b>
$N_{\max} = 2$	183.23	183.23	140.83	124.36	<b>121.33</b>
	138.98	138.10	98.46	98.46	<b>97.10</b>
$N_{\max} = 3$	184.91	184.91	165.23	97.05	<b>97.05</b>
	161.25	147.15	129.60	129.60	<b>126.77</b>
$\delta_{\max} = 4$	67.13	67.13	53.14	53.14	<b>53.00</b>
	85.77	85.77	64.11	66.11	<b>64.11</b>
$\delta_{\max} = 6$	111.18	70.11	70.11	70.11	<b>69.67</b>
	154.50	173.12	71.91	71.91	<b>69.43</b>
$\delta_{\max} = 8$	188.40	193.37	90.59	90.59	<b>89.67</b>
	185.18	189.28	122.25	124.94	<b>121.91</b>
$\delta_{\max} = 10$	171.23	194.10	80.60	89.43	<b>80.60</b>
	184.84	184.84	68.11	83.08	<b>68.11</b>

Table 2: Traversal costs using different policies (for illustration, we only show 2 cases for each setting from 100 replications)

Setting		Greedy Policies		RCDP Policies					Benchmark (Optimal)
$N_{\max}$	$n$	RD	DT	$r_{\delta}^L$	$r_{15}^L$	$r_{30}^L$	$r^{RD}$	$r^{DT}$	
1	20	0.26	0.20	0.75	0.54	0.35	0.24	0.19	0.32
	40	1.31	1.26	0.93	0.86	0.78	0.77	0.72	0.82
	80	2.00	1.87	0.73	0.38	0.18	0.07	0.03	0.09
2	20	0.26	0.20	1.09	0.62	0.38	0.26	0.20	0.34
	40	1.42	1.35	1.70	1.57	1.37	1.30	1.26	1.33
	80	2.96	2.75	1.60	0.78	0.37	0.24	0.15	0.32
3	20	0.26	0.20	1.21	0.63	0.28	0.26	0.20	0.34
	40	1.42	1.36	2.25	1.89	1.53	1.42	1.34	1.43
	80	3.82	3.54	2.52	1.47	0.80	0.74	0.54	0.70

(a) Results for  $N_{\max}$  values of 1, 2 and 3

Setting		Greedy Policies		RCDP Policies					Benchmark (Optimal)
$\delta_{\max}$	$n$	RD	DT	$r_{\delta}^L$	$r_{15}^L$	$r_{30}^L$	$r^{RD}$	$r^{DT}$	
4	20	1.14	1.16	2.92	1.66	1.04	1.10	0.84	1.54
6	20	1.16	0.84	3.38	1.80	1.12	1.14	0.85	1.66
	40	4.38	3.74	5.04	3.78	3.58	3.72	3.30	4.04
8	40	4.60	3.62	6.46	4.54	3.78	4.50	3.60	5.04
	80	8.82	8.72	7.8	5.46	4.26	5.78	4.42	6.50
10	80	9.56	9.38	9.72	8.72	7.40	8.92	8.78	9.00

(b) Results for  $\delta_{\max}$  values of 4, 6, 8 and 10

Table 3: The average number of intersected obstacles  $\bar{N}_p$  and the average resource needed  $\bar{\delta}_p$  on the traversal path  $p$  generated two greedy policies, five RCDP policies with different risk functions, and the benchmark policy

RCDP policies also intersect fewer true obstacles and require lower disambiguation costs on average. Greedy policies often violate budget constraints, particularly in dense environments, as evident from consistently higher average  $\bar{N}_p$  and  $\bar{\delta}_p$  values.

### 5.3 Summary of Key Empirical Findings

**Linear Undesirability (LU) Policies:** RCDP variants with LU risk functions—both fixed ( $\alpha = 15, 30$ ) and adaptive ( $\alpha = \delta_x$ )—consistently yield lower mean traversal costs and reduced variability compared to greedy baselines. No single  $\alpha$  value dominates across all settings, but  $\alpha = 15$  often achieves a favorable trade-off between risk aversion and exploration. Further simulation experiments (see Appendix Section A4.3) validate that a Bayesian version of the undesirability function, denoted  $r^{LB}$ , provides improved performance and asymptotic convergence to the benchmark as sensor precision improves.

**Reset Disambiguation (RD) and Distance-to-Termination (DT) Risk:** RCDP policies using these risk functions exhibit competitive performance, with the reset variant ( $r^{RD}$ ) often outperforming others in sparse and moderately dense environments. The DT variant performs better under generous budgets but degrades under tight constraints.

**Greedy Baselines:** Both constrained RD and DT policies frequently violate the disambiguation budget, especially in dense settings. Their lack of integrated budget reasoning leads to higher traversal cost, greater variability, and in some cases, longer-than-optimal detours.

**Budget Impact:** Increasing the disambiguation budget generally reduces traversal cost and error, while performance gaps between policies widen under tighter constraints. RCDP policies maintain constraint compliance and outperform greedy counterparts even under severe budget limitations.

**Robustness and Percentile Behavior:** RCDP policies demonstrate better performance not only on average but also in worst-case (75th percentile) and favorable (25th percentile) scenarios. This robustness is particularly pronounced in obstacle-dense environments ( $n = 80$ ).

In addition to average cost, RCDP policies also demonstrate superior robustness under uncertainty. Their traversal cost distributions exhibit lower standard deviation and narrower confidence intervals than greedy baselines, as seen in Appendix Figures A7-A9. Notably, their 75th percentile cost remains bounded even under high obstacle density and tight budgets, suggesting consistent performance in worst-case scenarios.

### 5.4 Evaluation of Policy Robustness

We assess policy robustness via *relative efficiency*, defined as:

$$\text{Efficiency}(r) = \frac{\mathcal{C}_{\text{offline}}}{\mathcal{C}_r},$$

where  $\mathcal{C}_{\text{offline}}$  is the expected cost under full obstacle knowledge, and  $\mathcal{C}_r$  is the average cost under risk model  $r$ .

Relative efficiency offers a normalized performance comparison against an idealized offline solution. We compute this metric across all simulation regimes and for each risk-based policy variant.

A detailed box plot visualization of relative efficiency is provided in the Appendix (Figure A16). These results highlight that risk-aware path planning with adaptive disambiguation policies yields consistent improvements over naive baselines. While RD and DT serve specialized roles, LU-based policies—with either fixed or cost-weighted scaling—deliver the most balanced performance under realistic sensing and resource constraints.

Full simulation configurations, additional tables (e.g., mean and variance of  $\mathcal{C}_p$  across 15 regimes), runtime statistics, and complete visualizations are available in the Appendix.

## 6 Discussion and Conclusions

This paper addresses a resource-constrained generalization of the Random Disambiguation Path (RDP) problem, extending the classical Stochastic Obstacle Scene (SOS) framework to reflect realistic operational constraints. In the RDP setting, a navigating agent (NAVA) seeks an optimal route through a spatial domain populated with disk-shaped obstacles of uncertain blockage. The agent may actively query (disambiguate) obstacle status, but incurs a cost for doing so. Unlike earlier work that neglects or simplifies resource limitations, we introduce an explicit disambiguation budget, formulating the resulting *RDP with Constrained Disambiguation* (RCDP) problem as a *Weight Constrained Shortest Path Problem* (WCSPP).

Our contribution is twofold: a theoretical reformulation of RCDP into a constrained optimization framework, and a practical algorithmic solution that integrates cost approximation with constraint-aware search. We develop surrogate cost models based on additive risk functions, combining Euclidean path length with sensor-informed obstacle risk. These approximations allow the constrained problem to be approached via a Lagrangian relaxation method, transforming the hard constraint into a penalized objective. To accelerate computation while preserving optimality, we introduce a two-phase vertex elimination (TPVE) strategy, which prunes non-promising vertices through feasibility and dominance tests.

Empirical validation across diverse simulation regimes demonstrates that the proposed RCDP policies consistently outperform greedy baselines, yielding lower expected traversal costs and reduced variability. The comparative analysis spans multiple risk functions—Reset Disambiguation (RD), Distance-to-Termination (DT), and Linear Undesirability (LU)—and evaluates performance using average cost, error rates, variability measures, and quantile-based statistics. The LU-based policies, particularly those with moderate or cost-sensitive scaling, exhibit strong robustness across a wide range of obstacle densities and budget levels.

The proposed TPVE-enhanced Lagrangian framework not only improves runtime efficiency but often eliminates the duality gap altogether, delivering provably optimal solutions in practice. We further support these findings with theoretical guarantees, including complexity bounds, feasibility preservation, and dominance over baseline policies.

**Limitations and Future Work.** Despite the effectiveness of our approach, several avenues remain open for further exploration: (i) **Multi-constraint extension:** Incorporating multiple disambiguation budgets (e.g., time, energy, or risk exposure) transforms the problem into a multi-dimensional WCSPP, necessitating new algorithmic designs. (ii) **Correlated obstacle statuses:** Our current model assumes independence across obstacles. Future work could explore spatial dependency structures (e.g., Markov random fields) and adapt pathfinding policies accordingly. (iii) **General obstacle geometries:** We currently model obstacles as uniform disks with binary status. More nuanced models could include irregular shapes or continuous risk fields, capturing partial blockage. (iv) **Dynamic and adversarial environments:** Introducing moving or adversarial obstacles would align the model with real-time navigation scenarios and call for adaptive or online decision-making under uncertainty. (v) **Tuning the  $\alpha$  parameter for linear undesirability (LU) risk function:** While this study employs a fixed linear undesirability

(LU) risk function with manually selected  $\alpha$ , we have explored data-driven strategies for tuning  $\alpha$  and adapting it through a Bayesian adjustment based on prior information about obstacle types and sensor accuracy. Although these extensions were not incorporated into the core simulation experiments, they offer a principled mechanism to enhance adaptability and robustness across diverse environments. The methodological details and empirical illustrations are provided in the Appendix (Section A3). Incorporating these adaptive risk formulations into future simulation pipelines remains a promising direction.

Overall, this work bridges constrained optimization, probabilistic reasoning, and graph-based navigation in uncertain environments. The RCDP formulation and solution framework offer a principled foundation for future developments in autonomous planning under partial observability and limited resources.

## Acknowledgements

Most of the Monte Carlo simulations presented in this article were executed at Easley HPC Laboratory of Auburn University. LZ and EC were supported by Office of Naval Research Grant N00014-22-1-2572 and EC were supported by NSF Award # 2319157.

## A1 Pseudocode for COGR and LOGR Algorithms

---

### Algorithm 4 Cost- and Obstacle-based Graph Reduction (COGR Algorithm)

---

**Input:** A graph with adjusted costs and weights  $G_{adj}$  from GI Algorithm, the start vertex  $s$ , the target vertex  $t$ , the disambiguation budget  $\delta_{\max}$

**Output:** Reduced graph  $G_{\text{red}}$ , optimal path  $p^*$  (or path with the lowest upper bound  $p_U$  and path with the highest lower bound  $p_L$ )

- 1: Initialize  $V_{\text{del}} \leftarrow \emptyset$  and  $E_{\text{del}} \leftarrow \emptyset$
- 2: Find the shortest obstacle-free path  $p^\infty$  using Dijkstra's algorithm with  $\lambda = \infty$
- 3: Find the minimum cost path  $p^0$  using Dijkstra's algorithm with  $\lambda = 0$
- 4: **if**  $\delta^0 \leq \delta_{\max}$  **then**
- 5:     **Output**  $p^* = p^0$ , **STOP**
- 6: **end if**
- 7:  $\tilde{\mathcal{C}}_U \leftarrow \tilde{\mathcal{C}}^\infty$ ;  $p_U \leftarrow p^\infty$
- 8: **repeat**
- 9:     **for**  $v \in V(G_{adj})$  **do**
- 10:         Find paths  $p_v^\infty$  and  $p_v^0$  through  $v$  with updated costs and weights
- 11:         **if**  $\delta_v^\infty > \delta_{\max}$  **then**
- 12:              $V_{\text{del}} \leftarrow V_{\text{del}} \cup \{v\}$
- 13:              $E_{\text{del}} \leftarrow E_{\text{del}} \cup \{e : e \text{ is incident to } v\}$
- 14:              $G_{adj} \leftarrow (V \setminus V_{\text{del}}, E \setminus E_{\text{del}})$
- 15:         **else if**  $\tilde{\mathcal{C}}_v^\infty < \tilde{\mathcal{C}}_U$  **then**
- 16:              $\tilde{\mathcal{C}}_U \leftarrow \tilde{\mathcal{C}}_v^\infty$ ;  $p_U \leftarrow p_v^\infty$
- 17:             Find  $p_v^0$  through  $v$  with updated costs and weights
- 18:             **if**  $\tilde{\mathcal{C}}_v^0 < \tilde{\mathcal{C}}_U$  and  $\delta_v^0 \leq \delta_{\max}$  **then**
- 19:                  $\tilde{\mathcal{C}}_U \leftarrow \tilde{\mathcal{C}}_{st,v}^0$ ;  $p_U \leftarrow p_v^0$
- 20:             **else if**  $\tilde{\mathcal{C}}_v^0 > \tilde{\mathcal{C}}_U$  **then**
- 21:                  $V_{\text{del}} \leftarrow V_{\text{del}} \cup \{v\}$
- 22:                  $E_{\text{del}} \leftarrow E_{\text{del}} \cup \{e : e \text{ is incident to } v\}$
- 23:                  $G_{adj} \leftarrow (V \setminus V_{\text{del}}, E \setminus E_{\text{del}})$
- 24:             **end if**
- 25:         **end if**
- 26:     **end for**
- 27: **until**  $V_{\text{del}} = \emptyset$
- 28:  $p^0 \leftarrow \min_v p_v^0$ ;  $p^\infty \leftarrow \min_v p_v^\infty$
- 29: **if**  $\delta^0 \leq \delta_{\max}$  **then**
- 30:     **Output**  $\{p^* = p^0\}$
- 31: **else**
- 32:     **Output**  $\{p_U = p^\infty, p_L = p^0\}$
- 33: **end if**

---

---

**Algorithm 5 Lagrangian Optimization and Graph Reduction (LOGR Algorithm)**


---

**Input:** The reduced-size graph  $G_{\text{red}}$ , path with the smallest upper bound  $p_U = p^\infty$ , path with the greatest lower bound  $p_L = p^0$ , the disambiguation budget  $\delta_{\text{max}}$

**Output:** Optimal path (or approximately optimal path)  $p^*$

- 1: Initialize  $i \leftarrow 0$
- 2: Set initial bounds:  $\tilde{\mathcal{C}}_i^+ \leftarrow \tilde{\mathcal{C}}_L$ ;  $\delta_i^+ \leftarrow \delta_L$ ;  $\tilde{\mathcal{C}}_i^- \leftarrow \tilde{\mathcal{C}}_U$ ;  $\delta_i^- \leftarrow \delta_U$
- 3: **while**  $p^*$  is not found **do**
- 4:    $\lambda_{i+1} \leftarrow \frac{\tilde{\mathcal{C}}_i^- - \tilde{\mathcal{C}}_i^+}{\delta_i^+ - \delta_i^-}$
- 5:   Find  $p_{i+1}$  in  $G_{\text{red}}$  with cost  $\tilde{\mathcal{C}}_{i+1} + \lambda_{i+1}\delta_{i+1}$
- 6:   **if**  $\delta_{i+1} = \delta_{\text{max}}$  **then**
- 7:     **Output**  $p^* = p_{i+1}$ , **break**
- 8:   **end if**
- 9:   **for**  $v \in V(G_{\text{red}})$  **do**
- 10:     Find  $p_{i+1,v}$  via  $v$
- 11:     **if**  $\tilde{\mathcal{C}}_{i+1,v} < \tilde{\mathcal{C}}_U$  and  $\delta_{i+1,v} \leq \delta_{\text{max}}$  **then**
- 12:        $\tilde{\mathcal{C}}_U \leftarrow \tilde{\mathcal{C}}_{i+1,v}$ ;  $p_U \leftarrow p_{i+1,v}$
- 13:     **end if**
- 14:     **if**  $\Phi(\lambda_{i+1}, p_{i+1,v}) > \tilde{\mathcal{C}}_U$  **then**
- 15:        $V_{\text{del}} \leftarrow V_{\text{del}} \cup \{v\}$
- 16:        $E_{\text{del}} \leftarrow E_{\text{del}} \cup \{e : e \text{ is incident to } v\}$
- 17:     **end if**
- 18:   **end for**
- 19:    $\tilde{\mathcal{C}}_L \leftarrow \min_{v \notin V_{\text{del}}} \Phi(\lambda_{i+1}, p_{i+1,v})$
- 20:   **if**  $\tilde{\mathcal{C}}_L = \tilde{\mathcal{C}}_U$  or  $\tilde{\mathcal{C}}_{i+1} + \lambda_{i+1}\delta_{i+1} = \tilde{\mathcal{C}}_i^+ + \lambda_{i+1}\delta_i^+$  (or  $\tilde{\mathcal{C}}_{i+1} + \lambda_{i+1}\delta_{i+1} = \tilde{\mathcal{C}}_i^- + \lambda_{i+1}\delta_i^-$ ) **then**
- 21:     **Output**  $p^* = p_U$ , **break**
- 22:   **end if**
- 23:    $G_{\text{red}} \leftarrow (V \setminus V_{\text{del}}, E \setminus E_{\text{del}})$
- 24:   **if**  $\delta_{i+1} < \delta_{\text{max}}$  **then**
- 25:     Update:  $\tilde{\mathcal{C}}_{i+1}^- \leftarrow \tilde{\mathcal{C}}_{i+1}$ ,  $\delta_{i+1}^- \leftarrow \delta_{i+1}$
- 26:   **else**
- 27:     Update:  $\tilde{\mathcal{C}}_{i+1}^+ \leftarrow \tilde{\mathcal{C}}_{i+1}$ ,  $\delta_{i+1}^+ \leftarrow \delta_{i+1}$
- 28:   **end if**
- 29: **end while**

---

## A2 Proofs of Main Theoretical Results

### A2.1 Cut-Based Cost Bounds

#### Proof of Property 3.1

*Proof.* Let  $\mathcal{S}_{\text{min}}$  be a minimum cardinality  $(s, t)$ -vertex cut in  $G$ . By definition, any path  $p \in \mathcal{P}(s, t)$  must pass through at least one vertex in  $\mathcal{S}_{\text{min}}$ . Therefore, the cost of the optimal constrained path  $p^*$  satisfies:

$$\tilde{\mathcal{C}}^* \geq \min_{\substack{p \in \mathcal{P}(s, t) \\ p \cap \mathcal{S}_{\text{min}} \neq \emptyset}} \tilde{\mathcal{C}}_p^0,$$

as this cost must be no less than that of the best unconstrained path through the cut.

For the upper bound, suppose there exists a feasible path  $p^\dagger$  with  $\delta_{p^\dagger} \leq \delta_{\text{max}}$ . Since  $p^\dagger$  must intersect  $\mathcal{S}_{\text{min}}$ , it follows that:

$$\tilde{\mathcal{C}}^* \leq \min_{\substack{p \in \mathcal{P}(s, t) \\ \delta_p \leq \delta_{\text{max}}, p \cap \mathcal{S}_{\text{min}} \neq \emptyset}} \tilde{\mathcal{C}}_p^\infty,$$

establishing the upper bound.

The cut  $\mathcal{S}_{\min}$  need not be unique. Any  $(s, t)$ -vertex cut suffices to derive valid bounds, though using a minimum cut often yields tighter estimates.

Finally, analogous arguments apply to edge cuts: one may replace  $\mathcal{S}_{\min}$  with a minimum set of edges that disconnect  $s$  from  $t$ , with the same bounding principles applied to edge-disjoint paths.  $\square$

## A2.2 Identification Results under Lagrangian Ambiguity

This section presents detailed proofs for Propositions 3.5–3.7, which establish the correctness of the TPVE algorithm under increasingly general disambiguation budget scenarios.

*Proof.* (Proof of Proposition 3.5) We begin by analyzing the feasibility of the three candidate paths:

- $p_1$  is infeasible since it intersects both obstacles and  $\delta_{p_1} = \delta_{x_1} + \delta_{x_2} > \delta_{\max}$ . Therefore, during Phase 1 of TPVE, any vertex  $v \in p_1$  lying in the intersection of  $x_1$  and  $x_2$  fails the feasibility test and is eliminated. Consequently,  $p_1$  is pruned.
- $p_2$  is feasible with  $\delta_{p_2} = 0$  and may appear attractive due to its low cost. However, if  $p^*$  has higher modified cost but better satisfies the constraint (i.e., utilizes part of the budget for informative disambiguation), then  $p_2$  cannot update the incumbent upper bound  $\tilde{\mathcal{C}}_U$ . Specifically, for any  $v \in p^* \setminus p_2$ , the shortest feasible path through  $v$  will necessarily involve  $x^*$  and yield cost  $\tilde{\mathcal{C}}_{p^*}$ , which defines  $\tilde{\mathcal{C}}_U$ .
- Since  $p^*$  intersects only one obstacle, say  $x^*$ , and satisfies  $\delta_{p^*} = \delta_{x^*} \leq \delta_{\max}$ , it passes the feasibility test. Furthermore, the dual cost  $\tilde{\mathcal{C}}_{p^*} + \lambda(\delta_{p^*} - \delta_{\max})$  can become optimal at some  $\lambda \geq 0$ , depending on the cost-risk tradeoff. In Phase 2, such vertices on  $p^*$  remain active, and the path  $p^*$  will be recovered either directly or as the vertex-constrained minimum modified cost path.

Thus, both  $p_1$  (infeasible) and  $p_2$  (suboptimal) are eliminated by the algorithm, while  $p^*$  survives and is ultimately selected as the optimal path. This concludes the proof.  $\square$

*Proof.* (Proof of Proposition 3.6) We proceed by induction on the number of obstacles  $k \geq 2$ .

**Base case ( $k = 2$ ):** This case corresponds to Proposition 3.5. Under the given assumptions, the TPVE algorithm eliminates the infeasible path (intersecting both obstacles) and the obstacle-free path (if suboptimal), and successfully identifies  $p^*$  as the unique feasible and optimal path.

**Inductive step:** Assume the proposition holds for  $k = m \geq 2$  obstacles. That is, if at most one obstacle can be disambiguated and a path  $p^*$  exists intersecting exactly one such obstacle while all competing paths either: (i) intersect multiple obstacles, making them infeasible, or (ii) avoid all obstacles but incur higher cost, then  $p^*$  is retained and identified by TPVE.

**Now consider  $k = m+1$  obstacles.** Let  $X = \{x_1, x_2, \dots, x_{m+1}\}$ , and suppose again that: -  $p^*$  intersects a single obstacle  $x^* \in X$  such that  $\delta_{x^*} \leq \delta_{\max}$ , - all other paths either intersect more than one obstacle (i.e.,  $\delta_p > \delta_{\max}$ ), or avoid all obstacles (i.e.,  $\delta_p = 0$  but  $\tilde{\mathcal{C}}_p > \tilde{\mathcal{C}}_{p^*}$ ).

Let  $V(p)$  denote the set of vertices on path  $p$ . During Phase 1 of TPVE: - All paths

that intersect multiple obstacles are pruned due to feasibility failure, and - All paths avoiding obstacles are retained but do not update the current upper bound  $\tilde{\mathcal{C}}_U = \tilde{\mathcal{C}}_{p^*}$ , since they are suboptimal.

During Phase 2: - Any vertex on  $p^*$  lies on a feasible path (namely,  $p^*$ ) whose cost equals the current best known cost  $\tilde{\mathcal{C}}_U$ . - Competing paths either do not improve the bound or are infeasible, hence do not eliminate vertices on  $p^*$ .

Thus, all non-optimal paths are eliminated by TPVE, while all vertices on  $p^*$  are retained. Therefore,  $p^*$  is preserved and ultimately identified as the optimal solution.

By the principle of mathematical induction, the result holds for all  $k \geq 2$ . □

*Proof.* (Proof of Proposition 3.7) We prove the claim by induction on the disambiguation budget parameter  $B \geq 1$ .

**Base case ( $B = 1$ ):** This corresponds to Proposition 3.6, already established. Under the assumptions, the TPVE algorithm prunes all infeasible or suboptimal paths and preserves  $p^*$ .

**Inductive step:** Suppose the result holds for disambiguation budgets up to  $B = m$  obstacles. That is, if a path  $p^*$  intersects at most  $m$  disjoint obstacles whose total disambiguation cost does not exceed  $\delta_{\max}$ , and all other paths either exceed budget or are cost-suboptimal, then TPVE preserves  $p^*$  and eliminates all competing paths.

**Now consider  $B = m + 1$ .** Let  $p^*$  intersect obstacles  $X^* = \{x_{i_1}, \dots, x_{i_{m+1}}\}$  such that:

$$\sum_{x \in X^*} \delta_x \leq \delta_{\max},$$

and  $p^*$  is the minimal-cost such feasible path.

During Phase 1 of TPVE:

- Any vertex  $v \in p^*$  belongs to a feasible path (namely  $p^*$ ). Since  $|X^*| = m + 1$  and the total cost of disambiguation is within budget, the feasibility test does not eliminate  $v$ .
- Any path  $p$  intersecting a set  $X_p$  of more than  $m + 1$  obstacles, or with  $\sum_{x \in X_p} \delta_x > \delta_{\max}$ , is deemed infeasible and eliminated.
- Any path avoiding all obstacles is retained, but does not improve the upper bound cost  $\tilde{\mathcal{C}}_U = \tilde{\mathcal{C}}_{p^*}$ .

During Phase 2:

- Since  $p^*$  is optimal and feasible under budget  $\delta_{\max}$ , its vertices remain in the graph.
- Competing paths that either violate feasibility or fail to improve the modified cost are not retained.

Thus,  $p^*$  is never eliminated and is ultimately selected by the algorithm.

By induction, the result holds for all  $B \geq 1$ . □

## A2.3 Spurious Dual Optima Vanish under High RBG

### Proof of Property 3.2

*Proof.* Suppose paths  $p_1$  and  $p_2$  satisfy conditions (i)–(iii). Let  $p^*$  be the optimal path, with cost  $\tilde{\mathcal{C}}^*$  and disambiguation cost  $\delta^* \leq \delta_{\max}$ .

From (iii), we have:

$$0 < \tilde{\mathcal{C}}_{p_2} - \tilde{\mathcal{C}}^* < \lambda^*(\delta^* - \delta_{p_2}),$$

implying that the apparent suboptimality of  $p_2$  is offset under the dual formulation by its lower disambiguation cost.

As RBG increases, the risk component  $r_p$  increases for any path intersecting uncertain obstacles. In particular, the gap  $r^* - r_{p_2}$  increases, and for sufficiently high RBG:

$$\ell_{p_2} - \ell^* < r^* - r_{p_2} \quad \Rightarrow \quad \tilde{\mathcal{C}}_{p_2} < \tilde{\mathcal{C}}^*,$$

contradicting the optimality of  $p^*$ .

For  $p_1$ , since it violates the disambiguation constraint ( $\delta_{p_1} > \delta_{\max}$ ), it is infeasible, yet (iii) implies:

$$0 < \lambda^*(\delta_{p_1} - \delta_{\max}) < \tilde{\mathcal{C}}^* - \tilde{\mathcal{C}}_{p_1}.$$

As RBG increases, so does  $r_{p_1}$  relative to  $r^*$ , and for large enough RBG:

$$\ell^* - \ell_{p_1} < r_{p_1} - r^* \quad \Rightarrow \quad \tilde{\mathcal{C}}_{p_1} < \tilde{\mathcal{C}}^*,$$

again contradicting optimality.

Thus, under high RBG, the coexistence of such dual-optimal but distinct paths becomes increasingly unlikely.  $\square$

## A2.4 Theorems and Propositions in Section 4.2

### Proof of Theorem 4.1

*Proof.* We divide the argument into two parts: feasibility and surrogate optimality.

**(i) Feasibility.** The COLOGR algorithm computes the optimal path over  $G_{\text{adj}}$  subject to the disambiguation constraint  $\delta_p \leq \delta_{\max}$ . This constraint is explicitly enforced during the graph reduction and optimization steps (e.g., via constrained Dijkstra variants). Thus, the selected solution  $p^*$  is guaranteed to be feasible.

**(ii) Surrogate Optimality.** Let  $\lambda^* \geq 0$  be the optimal Lagrange multiplier that maximizes the dual function:

$$\Phi(\lambda) = \min_{p \in \mathcal{P}(s,t;G_{\text{adj}})} \left\{ \tilde{\mathcal{C}}_p + \lambda(\delta_p - \delta_{\max}) \right\}.$$

Since  $\Phi(\lambda)$  is piecewise linear and concave, standard results from Lagrangian relaxation ensure that, if a path  $p^*$  is both feasible and achieves the dual minimum at  $\lambda^*$ , then

$$\tilde{\mathcal{C}}_{p^*} + \lambda^*(\delta_{p^*} - \delta_{\max}) = \Phi(\lambda^*).$$

Because  $\delta_{p^*} \leq \delta_{\max}$ , the penalty term vanishes, and  $p^*$  minimizes the surrogate cost over all feasible paths:

$$\tilde{\mathcal{C}}_{p^*} = \min \left\{ \tilde{\mathcal{C}}_p : p \in \mathcal{P}(s, t; G_{\text{adj}}), \delta_p \leq \delta_{\max} \right\}.$$

□

### A3 Tuning the Scaling Parameter $\alpha$ in the Linear Undesirability Function

To tailor traversal behavior to environmental uncertainty, we incorporate an  $\alpha$ -selection process into the policy. Since true obstacle status is unknown until disambiguation, each obstacle is modeled as a random variable with blockage probability  $\pi_x$ . Due to this stochasticity and the large number of obstacles, brute-force simulation across many  $\alpha$  values is impractical.

Instead, we investigate how the optimal  $\alpha$  varies with prior information accessible before traversal, including: (i) disambiguation resources  $\delta_x$ , (ii) the proportion  $\rho_T$  of true obstacles, and (iii) the probability distribution over obstacle types.

Assuming perfect sensing ( $\pi_x = 1$  for true,  $\pi_x = 0$  for false obstacles), true obstacles incur infinite penalty, while false obstacles ideally impose risk proportional to  $\delta_x$ . However, the standard linear undesirability function,

$$r_p^L = - \sum_{x \in X: p \cap x \neq \emptyset} \alpha \log(1 - \pi_x),$$

assigns negligible risk as  $\pi_x \rightarrow 0$ , underweighting the cost of false obstacle traversal. Thus, incorporating  $\delta_x$  into the base penalty yields a better approximation.

We assess how the optimal  $\alpha$  varies with  $\rho_T$ . Using the same simulation setup as in Section 5, we fix  $n = 20, 40, 80$  potential obstacles and vary  $\rho_T \in \{0, 0.1, 0.2, 0.4, 0.8, 1\}$ . Figure A5 shows the average traversal cost across 100 replications per setting.

As expected, traversal cost increases with  $\rho_T$  due to reduced path availability. Moreover, optimal  $\alpha$  also increases with  $\rho_T$ . When  $\rho_T$  is small, the constraint drives disambiguation selection toward low-risk paths, and a small  $\alpha$  suffices. As  $\rho_T$  rises, avoiding true obstacles becomes critical, and larger  $\alpha$  values are needed to accentuate risk differences.

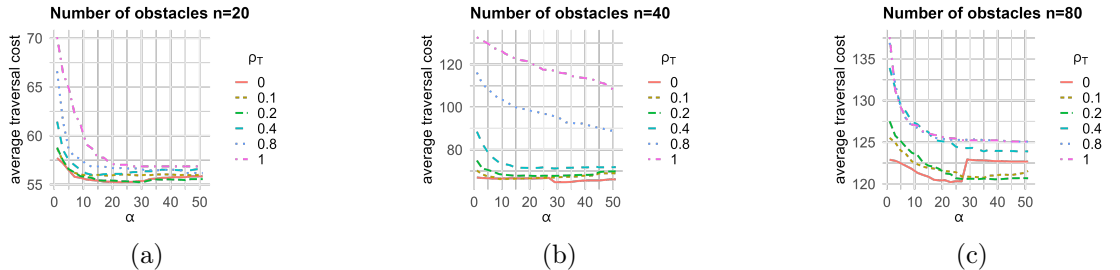


Figure A5: Effect of  $\alpha$  and true obstacle proportion  $\rho_T$  on mean traversal cost. Subplots: (a)  $n = 20$ , (b)  $n = 40$ , (c)  $n = 80$ .

To improve adaptivity, we propose a modified risk function:

$$r_p = \sum_{x \in X: p \cap x \neq \emptyset} (\delta_x - \alpha_x \log(1 - \pi_x)),$$

where  $\alpha_x$  is a local scaling parameter. This form satisfies  $r_p \rightarrow \sum \delta_x$  as  $\pi_x \rightarrow 0$ , ensuring alignment with disambiguation cost for low-risk obstacles.

The key challenge is determining  $\alpha_x$ . We propose a Bayesian framework that uses prior estimates of sensor reliability and obstacle prevalence to compute adjusted probabilities  $\pi_{x,\text{adj}}$ . Let  $\bar{\pi}$  denote the average prior probability of obstacles being true. If the sensor produces outputs drawn from  $f_T$  for true and  $f_F$  for false obstacles, then the adjusted probability becomes:

$$\pi_{x,\text{adj}} = P(f_T | \pi_x) = \frac{L(\pi_x | f_T) \cdot \bar{\pi}}{L(\pi_x | f_T) \cdot \bar{\pi} + L(\pi_x | f_F) \cdot (1 - \bar{\pi})}.$$

Assuming a preselected upper bound  $\alpha_{\max}$ , we set:

$$\alpha_x = \pi_{x,\text{adj}} \cdot \alpha_{\max},$$

yielding the Bayesian linear undesirability function:

$$r_p^{LB} = \sum_{x \in X: p \cap x \neq \emptyset} (\delta_x - \alpha_x \log(1 - \pi_x)).$$

This formulation improves traversal policy fidelity by modulating risk sensitivity based on both obstacle-level uncertainty and prior knowledge, with performance benefits validated in our simulations (Section A4.2).

### A3.1 Convergence to the Benchmark under Perfect Sensor Precision

We now show that the RCDP policy equipped with the Bayesian undesirability function asymptotically achieves the benchmark traversal cost as sensor accuracy becomes perfect.

**Theorem A3.1** (Convergence to Benchmark under Perfect Sensing). *Let  $\mathcal{C}_p^{LB}$  denote the traversal cost of the path selected by the RCDP policy using the Bayesian linear undesirability risk function  $r^{LB}$ , and let  $\mathcal{C}_p^{bm}$  denote the cost of the optimal path under perfect obstacle knowledge.*

*Assume:*

- (a) *Sensor probabilities converge pointwise:  $\pi_x \rightarrow \mathbb{I}\{x \in X_T\}$  for all  $x \in X$ .*
- (b)  *$\alpha_x$  is uniformly bounded and independent of  $\pi_x$ .*
- (c) *Edge lengths  $\ell_e$  and disambiguation costs  $\delta_e$  are fixed.*
- (d) *For all  $p$ , the actual traversal cost  $\mathcal{C}_p$  is bounded above.*

*Then:*

$$\mathbb{E}[\mathcal{C}_{p^{LB}}] \rightarrow \mathcal{C}_{p^{bm}},$$

*where  $p^{LB}$  is any path selected by the RCDP policy under  $r^{LB}$ .*

*Proof.* Let  $G = (V, E)$  denote the spatial graph. Under perfect sensing, edge costs become:

$$\mathcal{C}_e^{bm} = \begin{cases} \ell_e + \frac{1}{2} \sum_{x \in X_F: x \cap e \neq \emptyset} \delta_x, & \text{if } e \cap X_T = \emptyset, \\ \infty, & \text{otherwise.} \end{cases}$$

Now consider the Bayesian surrogate cost:

$$\tilde{\mathcal{C}}_e^{LB} = \ell_e + \frac{1}{2} \sum_{x \in X: x \cap e \neq \emptyset} (\delta_x - \alpha_x \log(1 - \pi_x)).$$

As  $\pi_x \rightarrow \mathbb{I}\{x \in X_T\}$ , we have: - For  $x \in X_T$ ,  $-\log(1 - \pi_x) \rightarrow \infty \Rightarrow \tilde{\mathcal{C}}_e^{LB} \rightarrow \infty$  if  $e$  intersects a true obstacle. - For  $x \in X_F$ ,  $-\log(1 - \pi_x) \rightarrow 0 \Rightarrow \tilde{\mathcal{C}}_e^{LB} \rightarrow \mathcal{C}_e^{bm}$ .

Hence,  $\tilde{\mathcal{C}}_e^{LB} \rightarrow \mathcal{C}_e^{bm}$  uniformly over  $e$ .

By continuity of path cost with respect to edge costs, this implies:

$$\tilde{\mathcal{C}}_p^{LB} \rightarrow \mathcal{C}_p^{bm} \quad \text{for all feasible paths } p.$$

The feasibility constraint  $\delta_p \leq \delta_{\max}$  remains unchanged, as it depends only on obstacle geometry.

Since the argmin over continuous and bounded costs is stable under uniform convergence (Berge's Maximum Theorem), the selected path  $p^{LB}$  satisfies:

$$\mathbb{E}[\mathcal{C}_{p^{LB}}] \rightarrow \mathcal{C}_{p^{bm}}.$$

□

Simulation results in Figure A13 support this convergence, showing that as sensor precision increases, the traversal cost under  $r^{LB}$  closely approximates the benchmark.

## A4 Details of the Monte Carlo Simulations

### A4.1 Graph Reduction Performance: TPVE vs. SNE

We conduct Monte Carlo simulations (1000 replications) to compare the performance of the proposed Two-Phase Vertex Elimination (TPVE) method with the original Simple Node Elimination (SNE). Table A4 reports results over all replications and for selected cases that exhibit either a nonzero duality gap or noticeable cost differences—highlighting meaningful distinctions between the two reduction strategies.

The simulation domain is  $\Omega = [0, 100] \times [0, 50]$  and contains 20, 40, or 80 disk-shaped obstacles, among which 4, 8, or 16 are true obstacles, respectively. The source and target are fixed at  $s = (50, 50)$  and  $t = (50, 1)$ , resulting in an initial graph with 5151 vertices.

To isolate the impact of graph reduction, we adopt the proposed traversal policy with the linear undesirability function ( $\alpha = 15, 30$ ) and consider both: (i) heterogeneous disambiguation costs, and (ii) a uniform cost setting where the constraint simplifies to a bound on the number of disambiguated obstacles.

Further simulation and policy comparisons are provided in Section A4.2.

As seen in Table A4, TPVE consistently produces smaller final graphs and closes the duality gap in all runs (gap = 0), while SNE shows a nonzero gap in aggregate and selected cases (e.g., 0.026 on average in selected cases). Although both methods sometimes yield paths with identical costs, SNE more frequently fails to identify the true optimal path due to suboptimal pruning. This results either from unresolved duality gaps or from ties in surrogate cost, where TPVE better captures the true optimum.

	Two-Phase Vertex Elimination (TPVE)			Simple Node Elimination (SNE)		
	Graph Size (number of vertices)	Duality Gap ( $\frac{\text{upper-lower}}{\text{lower}}$ )	$\mathcal{C}_p$	Graph Size (number of vertices)	Duality Gap ( $\frac{\text{upper-lower}}{\text{lower}}$ )	$\mathcal{C}_p$
Case 1	728	0	75.658	499	0.016	75.658
Case 2	136	0	58.490	4231	0.064	59.405
Case 3	158	0	62.450	278	0.023	62.450
Case 4	225	0	59.282	4213	0	63.090
Case 5	137	0	64.065	829	0.879	64.065
Average (50 selected cases)	142	0	57.304	3948	0.026	61.015
Average (1000 cases)	2423	0	58.444	3745	0.001	58.667

Table A4: Comparison of TPVE and SNE on final graph size, duality gap, and traversal cost.

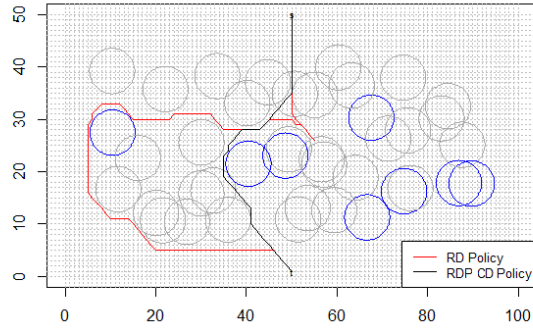
## A4.2 Comprehensive Comparisons of Traversal Policies

In this section, we provide a comprehensive comparison of the policies, including detailed analyses using the metrics introduced in Section 5 as well as additional evaluation metrics.

1. *Average traversal cost with confidence interval*: this primary metric measures the mean traversal cost from starting point to target point across different environments, directly reflects policy’s quality, where lower values indicate superior overall performance.
2. *Error relative to optimal*: calculated as  $\sqrt{\frac{\sum_i (\mathcal{C}_i - \mathcal{C}^*)^2}{n}}$ , where  $\mathcal{C}_i$  is the traversal cost in  $i^{\text{th}}$  simulation, quantifying the deviation from an optimal cost generated by an offline benchmark assuming perfect knowledge of obstacle status. This metric assesses how closely each policy approximates the idealized best scenario.
3. *Variability*: using standard deviation of traversal costs across different environments, reflecting each policy’s stability and reliability under varying uncertain conditions.
4. *Quantile metrics*: specifically, the 25<sup>th</sup> and 75<sup>th</sup> percentiles of traversal costs across different environments are analyzed to reveal performance under both favorable and challenging scenarios, offering additional insights into each policy’s robustness and consistency.

Together, these metrics provide comprehensive assessment of each policy’s strengths and weaknesses.

Figure A6 visualizes an example comparison under the simplified scenario with  $N_{\text{max}} = 2$ , contrasting the RCDP policy and the constrained RD policy.



(a)

Figure A6: Example traversal paths under  $N_{\max} = 2$  for RCDP and constrained RD policies.

Figure A7 shows the mean traversal cost with 95% confidence intervals for all policies. As expected, traversal cost increases with obstacle count due to greater obstruction, while larger disambiguation budgets yield lower costs by enabling more effective exploration and obstacle avoidance.

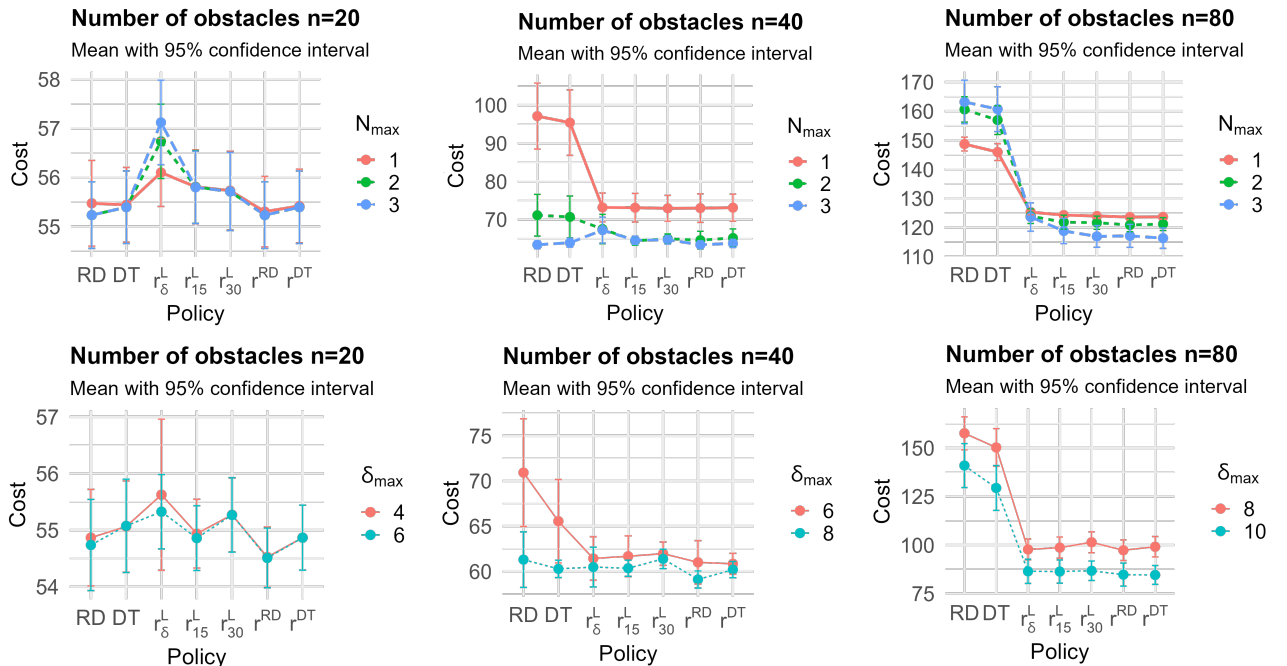


Figure A7: Average traversal cost with 95% confidence interval across two greedy policies and five RCDP policies using different risk functions.

The RCDP policies consistently outperform the constrained RD and DT baselines. This improvement stems from the RCDP's global consideration of the disambiguation budget, in contrast to the myopic cost-minimization strategy of greedy methods.

As obstacle density increases or disambiguation budgets become tighter, the performance

gap widens. RCDP policies exhibit both lower average cost and smaller confidence intervals, indicating greater robustness. In contrast, greedy policies sometimes exceed even the length of the longest obstacle-free path (150 units), a shortcoming not observed with RCDP.

These findings are further substantiated in Table A6, which records the average number of obstacles intersected (in the simplified scenario) and disambiguation cost used (in the general scenario). Greedy methods often breach the constraint, while RCDP policies remain feasible and efficient.

Figure A8 presents the standard deviations of traversal costs. Again, RCDP policies display smaller variability, reinforcing their consistency across heterogeneous environments.

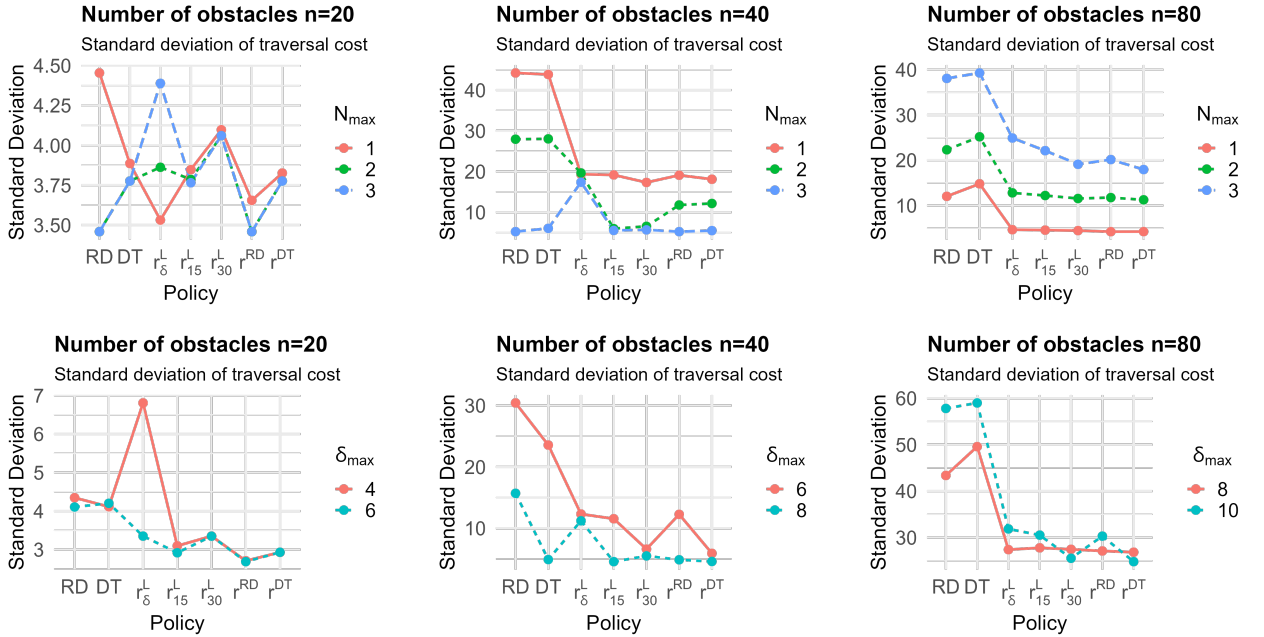


Figure A8: Standard deviation of traversal costs across policies and environments. Lower variance for RCDP policies indicates higher stability under uncertainty.

Figure A9 compares policies using the error metric, which captures the deviation of traversal cost from the offline optimal. As obstacle density increases and disambiguation budgets tighten, error magnitudes rise—reflecting the greater complexity of navigating such environments. Consistent with other performance metrics, RCDP policies achieve lower errors than greedy alternatives, especially under challenging conditions, highlighting their superior adaptivity and planning efficiency.

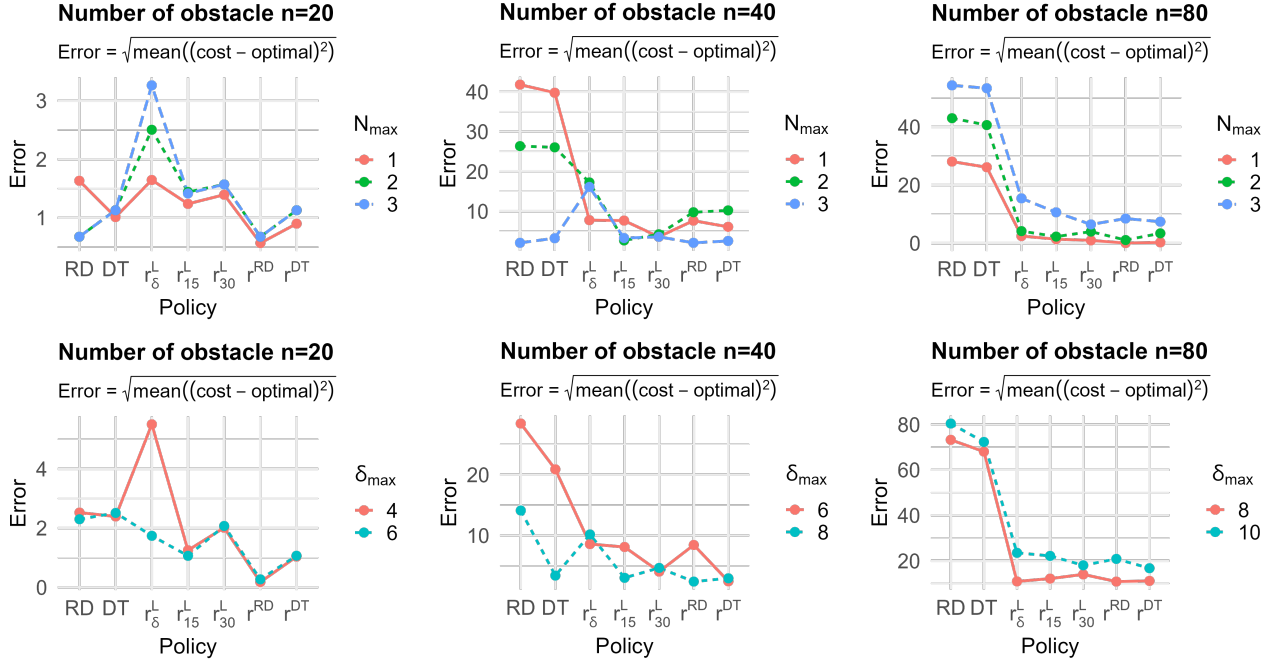


Figure A9: The deviation of two greedy policies, five RCDP policies with different risk functions from optimal solutions

Figures A10 and A11 show the 25<sup>th</sup> and 75<sup>th</sup> percentile traversal cost across environments, respectively, capturing each policy’s performance in relatively favorable and challenging conditions. Results regarding 25<sup>th</sup> percentile indicate that in less dense environments, policies show similar performance, but distinctions in policies’ performance become more obvious as obstacle density increases. Especially in environments with  $n = 80$ , greedy policies tend to show much higher variability in the 25<sup>th</sup> percentile compared to RCDP policies. This suggests that although greedy policies may find efficient paths, their lack of strategic disambiguation planning results in greater sensitivity to environment conditions. When we compare policies regarding 75<sup>th</sup> percentile, the benefits of applying RCDP policies compared to greedy policies become more evident. Greedy policies tend to exhibit higher 75<sup>th</sup> percentile traversal costs than RCDP policies, particularly in obstacle-dense environments ( $n = 80$ ). RCDP policies, in contrast, demonstrate better and more robust performance in worst scenarios, due to the systematic integration of risk into their entire decision-making process.

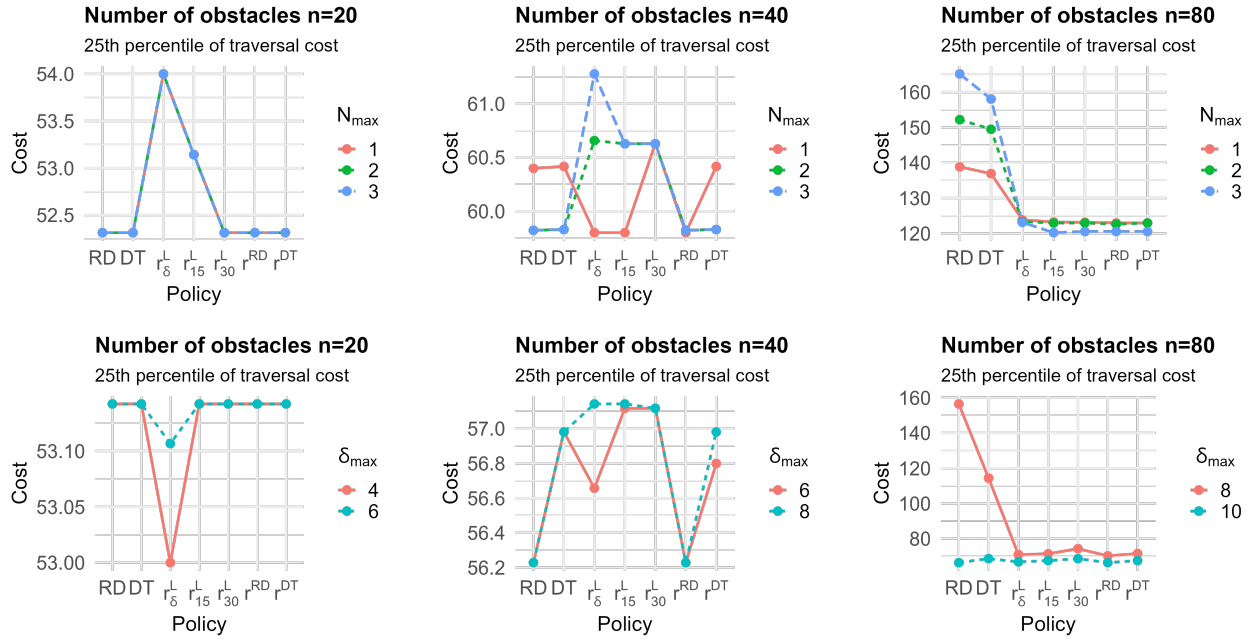


Figure A10: The 25<sup>th</sup> percentile of traversal costs across different environments using two greedy policies, five RCDP policies with different risk functions

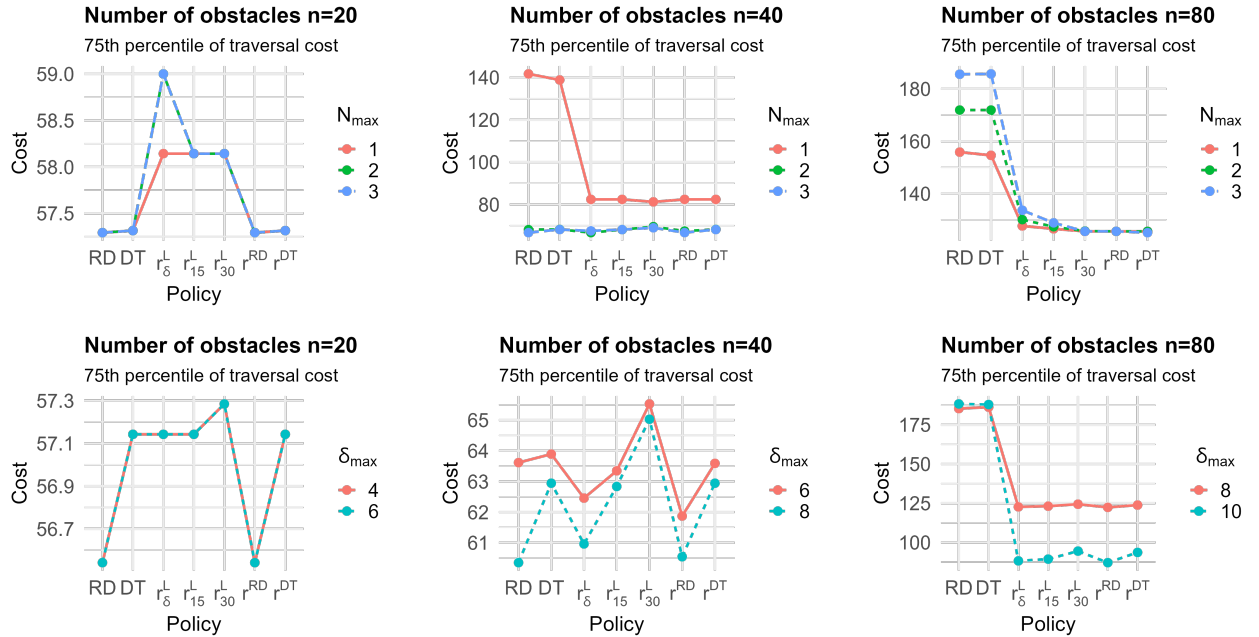


Figure A11: The 75<sup>th</sup> percentile of traversal costs across different environments using two greedy policies, five RCDP policies with different risk functions

In summary, RCDP policies consistently deliver more effective traversal performance than their greedy counterparts, particularly in complex and uncertain environments. Their advantage stems from a principled use of risk-aware planning under budget constraints, resulting in solutions that are not only cost-efficient but also stable across varying obstacle densities and risk profiles.

Setting	Greedy Policies					RCDP Policies										Benchmark (Optimal)	
	RD		DT		$\bar{C}_p$	$r_6^L$		$r_{15}^L$		$r_{30}^L$		$r^{RD}$		$r^{DT}$			
$N_{\max}$	$n$	$\bar{C}_p$	$SD(\mathcal{C}_p)$	$\bar{C}_p$		$SD(\mathcal{C}_p)$	$\bar{C}_p$	$SD(\mathcal{C}_p)$	$\bar{C}_p$	$SD(\mathcal{C}_p)$	$\bar{C}_p$	$SD(\mathcal{C}_p)$	$\bar{C}_p$	$SD(\mathcal{C}_p)$	$\bar{C}_p$	$SD(\mathcal{C}_p)$	$\bar{C}_p$
1	20	55.47	4.45	55.44	3.89	56.10	3.53	55.81	3.85	55.73	4.10	<b>55.30</b>	<b>3.65</b>	55.42	3.82	55.14	
	40	99.12	44.20	95.42	43.82	73.17	19.32	73.09	19.16	<b>72.95</b>	<b>17.32</b>	72.99	19.09	73.11	18.09	71.73	
	80	148.69	12.03	145.94	14.79	125.31	4.65	124.29	4.56	123.97	4.44	<b>123.62</b>	<b>4.22</b>	123.68	4.23	123.62	
2	20	55.23	3.46	55.39	3.78	56.73	3.86	55.81	3.79	55.71	4.06	<b>55.23</b>	<b>3.46</b>	55.39	3.78	55.05	
	40	71.72	27.92	70.68	28.01	67.51	19.64	<b>64.42</b>	<b>5.97</b>	64.96	6.54	64.61	11.77	65.16	12.15	62.91	
	80	160.58	22.31	156.91	25.18	123.91	12.79	121.86	12.20	121.67	11.55	<b>120.89</b>	<b>11.75</b>	121.20	11.26	120.74	
3	20	55.23	<b>3.46</b>	55.39	3.78	57.12	4.39	55.80	3.77	55.71	4.06	<b>55.23</b>	<b>3.46</b>	55.39	3.78	55.05	
	40	63.39	5.23	63.92	6.03	67.21	17.36	64.55	5.53	64.69	5.66	<b>63.39</b>	<b>5.23</b>	63.74	5.48	62.48	
	80	163.15	38.08	160.67	39.29	123.62	24.91	118.83	22.12	116.96	19.11	117.15	20.15	<b>116.36</b>	<b>17.94</b>	114.99	

Results for  $N_{\max}$  values of 1, 2, and 3

Setting	Greedy Policies					RCDP Policies										Benchmark (Optimal)	
	RD		DT		$\bar{C}_p$	$r_6^L$		$r_{15}^L$		$r_{30}^L$		$r^{RD}$		$r^{DT}$			
$\delta_{\max}$	$n$	$\bar{C}_p$	$SD(\mathcal{C}_p)$	$\bar{C}_p$		$SD(\mathcal{C}_p)$	$\bar{C}_p$	$SD(\mathcal{C}_p)$	$\bar{C}_p$	$SD(\mathcal{C}_p)$	$\bar{C}_p$	$SD(\mathcal{C}_p)$	$\bar{C}_p$	$SD(\mathcal{C}_p)$	$\bar{C}_p$	$SD(\mathcal{C}_p)$	$\bar{C}_p$
4	20	54.87	4.27	55.06	4.11	55.62	6.81	54.94	3.10	55.27	3.35	<b>54.52</b>	<b>2.71</b>	54.87	2.93	54.47	
	40	54.74	4.11	55.06	4.20	55.32	3.35	54.86	2.92	55.72	3.35	<b>54.51</b>	<b>2.69</b>	54.87	2.93	54.44	
6	20	70.54	29.93	65.44	23.30	61.42	12.31	61.66	11.54	61.95	6.60	60.99	12.26	<b>60.82</b>	<b>5.91</b>	59.67	
	40	61.25	15.45	60.24	4.33	60.47	11.21	60.33	4.56	61.37	5.49	<b>59.09</b>	<b>4.86</b>	60.18	4.58	58.49	
8	20	156.01	42.77	148.83	48.79	<b>97.21</b>	<b>27.41</b>	98.66	27.80	98.97	27.48	97.31	27.12	99.10	26.86	95.22	
	40	139.81	56.98	128.40	58.11	86.44	31.86	86.31	30.53	86.31	25.55	84.72	30.32	<b>84.56</b>	<b>24.82</b>	80.51	

Results for  $\delta_{\max}$  values of 4, 6, 8, and 10

Table A5: The average traversal costs  $\bar{C}_p$  and standard deviation  $SD(\mathcal{C}_p)$  of two greedy policies, five RCDP policies with different risk functions, and the benchmark policy.

Setting		Greedy Policies		RCDP Policies					Benchmark (Optimal)
$N_{\max}$	$n$	RD	DT	$r_{\delta}^L$	$r_{15}^L$	$r_{30}^L$	$r^{RD}$	$r^{DT}$	
1	20	0.26	0.20	0.75	0.54	0.35	0.24	0.19	0.32
	40	1.31	1.26	0.93	0.86	0.78	0.77	0.72	0.82
	80	2.00	1.87	0.73	0.38	0.18	0.07	0.03	0.09
2	20	0.26	0.20	1.09	0.62	0.38	0.26	0.20	0.34
	40	1.42	1.35	1.70	1.57	1.37	1.30	1.26	1.33
	80	2.96	2.75	1.60	0.78	0.37	0.24	0.15	0.32
3	20	0.26	0.20	1.21	0.63	0.28	0.26	0.20	0.34
	40	1.42	1.36	2.25	1.89	1.53	1.42	1.34	1.43
	80	3.82	3.54	2.52	1.47	0.80	0.74	0.54	0.70

(a) Results for  $N_{\max}$  values of 1, 2 and 3

Setting		Greedy Policies		RCDP Policies					Benchmark (Optimal)
$\delta_{\max}$	$n$	RD	DT	$r_{\delta}^L$	$r_{15}^L$	$r_{30}^L$	$r^{RD}$	$r^{DT}$	
4	20	1.14	1.16	2.92	1.66	1.04	1.10	0.84	1.54
6	20	1.16	0.84	3.38	1.80	1.12	1.14	0.85	1.66
	40	4.38	3.74	5.04	3.78	3.58	3.72	3.30	4.04
8	40	4.60	3.62	6.46	4.54	3.78	4.50	3.60	5.04
	80	8.82	8.72	7.8	5.46	4.26	5.78	4.42	6.50
10	80	9.56	9.38	9.72	8.72	7.40	8.92	8.78	9.00

(b) Results for  $\delta_{\max}$  values of 4, 6, 8 and 10

Table A6: The average number of intersected obstacles  $\bar{N}_p$  and the average resource needed  $\bar{\delta}_p$  on the traversal path  $p$  generated two greedy policies, five RCDP policies with different risk functions, and the benchmark policy

RCDP policies also intersect fewer true obstacles and require lower disambiguation costs on average. Greedy policies often violate budget constraints, particularly in dense environments, as evident from consistently higher average  $\bar{N}_p$  and  $\bar{\delta}_p$  values.

### A4.3 Efficacy of the Bayesian Linear Undesirability Function

To further assess the efficacy of the Bayesian linear undesirability function, we evaluate its performance relative to other risk models using simulations across varying obstacle densities, proportions of true obstacles, and sensor accuracies. We focus on how performance varies with: (i) the number of obstacles  $n$  and true obstacle ratio  $\rho_T$ , (ii) the precision of sensor-derived probabilities  $\pi_x$ , and (iii) the underlying spatial distribution of obstacles.

#### A4.3.1 Sensitivity to the Proportion of True Obstacles

Using the simulation setup described in Section 5, we analyze traversal performance across  $\rho_T \in \{0, 0.1, 0.2, 0.4, 0.8, 1\}$  and for  $n = 20, 40, 80$  obstacles. We set  $\alpha_{\max} = 60$  in the Bayesian risk function.

Figure A12 shows the average traversal cost under six risk functions. The Bayesian undesirability function consistently achieves the lowest mean cost, particularly as  $\rho_T$  increases—highlighting its improved risk discrimination and path planning under elevated uncertainty.

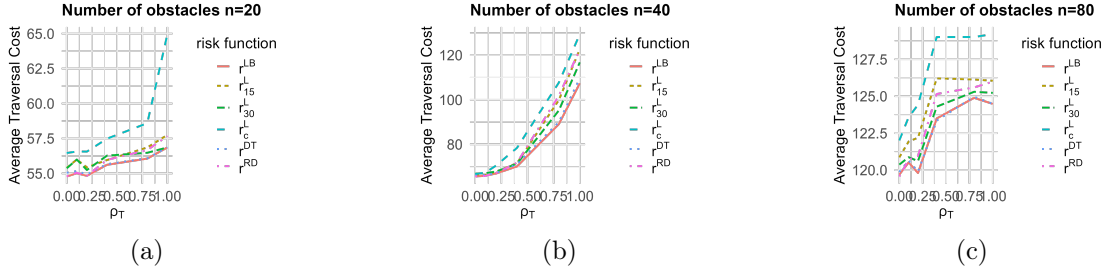


Figure A12: Traversal cost versus true obstacle proportion  $\rho_T$  using six different risk functions. Panels: (a)  $n = 20$ , (b)  $n = 40$ , (c)  $n = 80$ .

Beyond mean performance, we also assess how often each policy achieves the minimum cost within individual replications. Table A7 reports the proportion of 100 simulations in which the Bayesian risk function ( $r^{LB}$ ) outperforms all others. It dominates consistently—especially in high  $\rho_T$  settings and under simplified constraints—confirming its robustness in both average-case and worst-case conditions.

		$n = 20$					
$\rho_T$		0	0.1	0.2	0.4	0.8	1
Simplified Scenario ( $N_{\max}$ )		0.98	0.97	0.97	0.98	0.98	1.00
General Scenario ( $\delta_{\max}$ )		0.81	0.77	0.80	0.91	0.92	1.00
		$n = 40$					
$\rho_T$		0	0.1	0.2	0.4	0.8	1
Simplified Scenario ( $N_{\max}$ )		0.94	0.90	0.92	0.87	0.92	0.91
General Scenario ( $\delta_{\max}$ )		0.56	0.58	0.59	0.58	0.84	0.93
		$n = 80$					
$\rho_T$		0	0.1	0.2	0.4	0.8	1
Simplified Scenario ( $N_{\max}$ )		0.96	0.97	0.98	0.98	0.99	1.00
General Scenario ( $\delta_{\max}$ )		0.62	0.55	0.57	0.56	0.84	1.00

Table A7: Proportion of simulations in which the Bayesian linear undesirability function yields the lowest traversal cost.

### A4.3.2 Impact of Sensor Accuracy on Traversal Cost

To further evaluate the convergence behavior of the RCDP policy with the Bayesian undesirability function  $r^{LB}$ , we empirically assess how traversal cost evolves with increasing sensor precision. As established in Theorem A3.1,  $r^{LB}$  approximates the benchmark cost under perfect sensing. Here, we validate this convergence across a continuum of sensor accuracies.

Using the same simulation setup as in Sections 5 and A4.3.1, we vary a proxy parameter  $\lambda$  controlling the sensor’s informativeness over the range  $[0, 4]$  in increments of 0.5. For each setting, we simulate 100 replications and compute the mean traversal cost under the RCDP policy with  $r^{LB}$ , denoted  $\bar{\mathcal{C}}_{p^{LB}}$ , and compare it to the benchmark cost  $\bar{\mathcal{C}}_{p^{bm}}$ .

Figure A13 shows that  $\bar{\mathcal{C}}_{p^{LB}}$  decreases monotonically as  $\lambda$  increases, aligning with prior

findings that higher sensor precision improves policy performance (Ye et al., 2011). For  $\lambda \geq 3$ , the cost closely matches the benchmark, indicating practical convergence even under moderately accurate sensors.

This monotonicity not only reinforces theoretical guarantees but also demonstrates that  $r^{LB}$  provides an effective, adaptive framework in settings with evolving or imperfect sensor inputs.

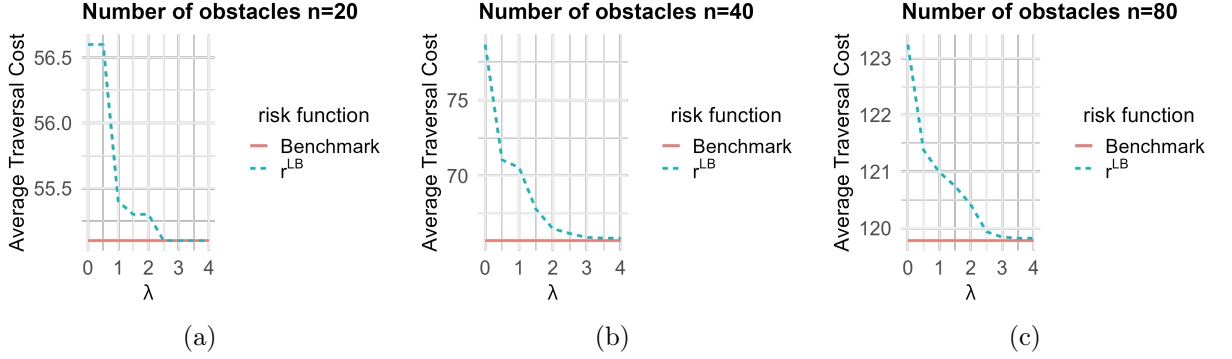


Figure A13: Traversal cost under the RCDP policy with  $r^{LB}$  versus benchmark cost, as a function of sensor precision  $\lambda$ . Panels: (a)  $n = 20$ , (b)  $n = 40$ , (c)  $n = 80$ .

#### A4.3.3 Effect of Obstacle Spatial Pattern on Pathfinding Performance

To test the robustness of our findings under alternative spatial assumptions, we replicate the experiments from Sections A4.3.1 and A4.3.2 using two different obstacle placement processes: (i) a uniform point process, and (ii) a Matérn clustering point process.

All other parameters are held constant to isolate the effect of spatial patterning. Figures A14 and A15 show that the RCDP policy with  $r^{LB}$  retains its performance advantage across both spatial patterns. Its superior adaptivity and convergence to benchmark performance are consistent with results under Strauss-based configurations.

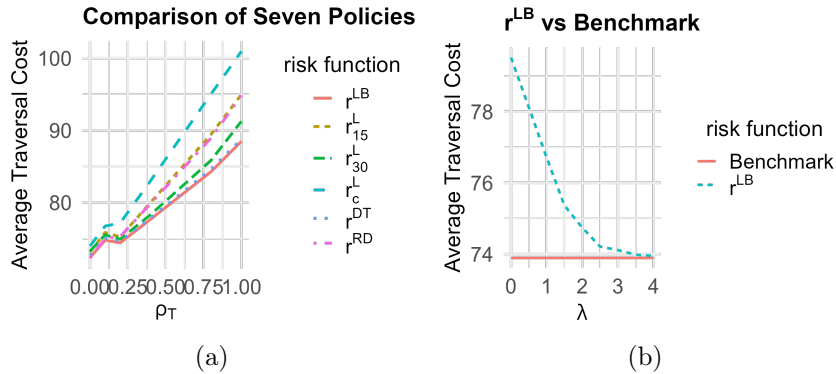


Figure A14: RCDP policy with  $r^{LB}$  under uniform obstacle placement: (a) traversal cost versus proportion of true obstacles; (b) cost comparison with benchmark versus sensor accuracy  $\lambda$ .

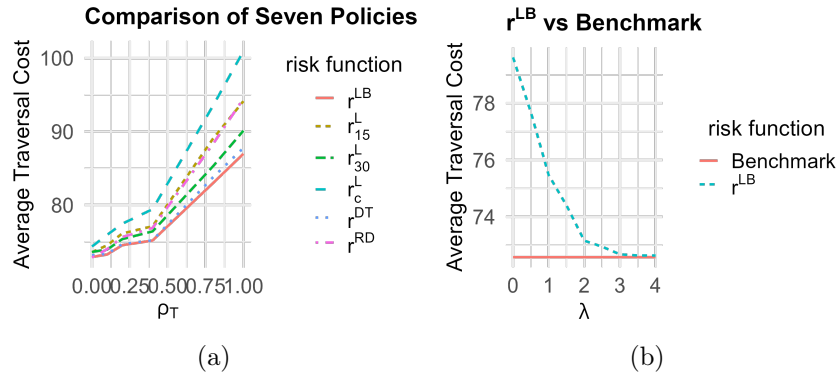


Figure A15: RCDP policy with  $r^{LB}$  under clustered (Matérn) obstacle placement: (a) traversal cost versus proportion of true obstacles; (b) cost comparison with benchmark versus sensor accuracy  $\lambda$ .

#### A4.4 Visualization of Relative Efficiency

Figure A16 presents the relative efficiency box plots for each policy across 15 simulation regimes. LU-based policies consistently achieve high median efficiency with tight variance, indicating robust performance under diverse environment and sensing settings.

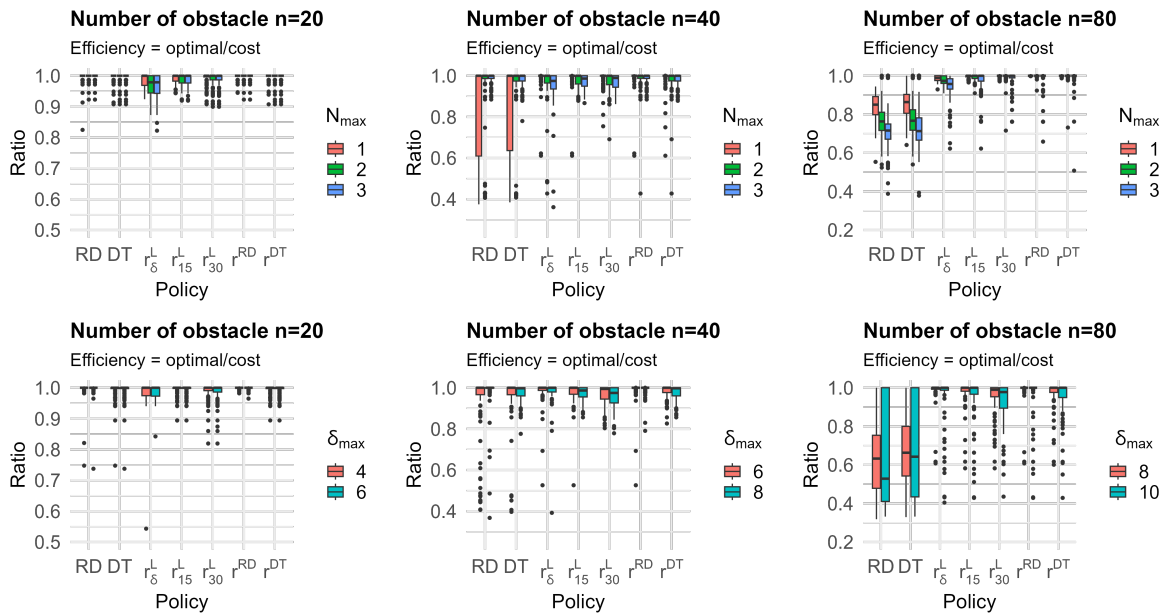


Figure A16: Relative efficiency of risk-based RCDP policies aggregated over all 15 simulation regimes. LU policies achieve high median efficiency with tight variance.

## References

Aksakalli, V. and Ari, I. (2014). Penalty-based algorithms for the stochastic obstacle scene problem. *INFORMS Journal on Computing*, 26:370–384.

- Aksakalli, V., Fishkind, D. E., Priebe, C. E., and Ye, X. (2011). The reset disambiguation policy for navigating stochastic obstacle fields. *Naval Research Logistics*, 58(4):389–399.
- Aksakalli, V., Sahin, O. F., and Ari, I. (2016). An AO\* based exact algorithm for the Canadian traveler problem. *INFORMS Journal on Computing*, 28(1):96–111.
- Alkaya, A. F. and Algin, R. (2015). Metaheuristic based solution approaches for the obstacle neutralization problem. *Expert systems with applications*, 42(3):1094–1105.
- Alkaya, A. F., Yildirim, S., and Aksakalli, V. (2021). Heuristics for the Canadian traveler problem with neutralizations. *Computers & Industrial Engineering*, 159:107488.
- Azizi, E. and Seifi, A. (2024). Shortest path network interdiction with incomplete information: a robust optimization approach. *Annals of Operations Research*, 335(2):727–759.
- Baddeley, A. (2010). Analysing spatial point patterns in R. *Workshop notes Ver. 4.1*.
- Dijkstra, E. W. (1959). A note on two problems in connexion with graphs. *Numerische Mathematik*, 1(1):269–271.
- Fishkind, D. E., Priebe, C. E., Giles, K., Smith, L. N., and Aksakalli, V. (2007). Disambiguation protocols based on risk simulation. *IEEE Transactions on Systems, Man, and Cybernetics*, 37(5):814–823.
- Guo, L. and Matta, I. (2003). Search space reduction in QoS routing. *Computer Networks*, 41(1):73–88.
- Israeli, E. and Wood, R. K. (2002). Shortest-path network interdiction. *Networks: An International Journal*, 40(2):97–111.
- Jüttner, A. (2005). On resource constrained optimization problems. In *4th Japanese-Hungarian Symposium on Discrete Mathematics and Its Applications*, pages 3–6.
- Juttner, A., Szviatovski, B., Mecs, I., and Rajko, Z. (2001). Lagrange relaxation based method for the QoS routing problem. In *Proceedings IEEE INFOCOM 2001. Conference on Computer Communications. Twentieth Annual Joint Conference of the IEEE Computer and Communications Society (Cat. No.01CH37213)*, volume 2, pages 859–868 vol.2.
- Muhandiramge, R. and Boland, N. (2009). Simultaneous solution of Lagrangean dual problems interleaved with preprocessing for the weight constrained shortest path problem. *Networks*, 53:358–381.
- Papadimitriou, C. H. and Yannakakis, M. (1991). Shortest paths without a map. *Theoretical Computer Science*, 84(1):127–150.
- Priebe, C., Fishkind, D., Abrams, L., and Piatko, C. (2005). Random disambiguation paths for traversing a mapped hazard field. *Naval Research Logistics (NRL)*, 52:285 – 292.
- Sadeghi, S. and Seifi, A. (2024). A modified scenario bundling method for shortest path network interdiction under endogenous uncertainty. *Annals of Operations Research*, pages 1–29.
- Smith, J. C. and Song, Y. (2020). A survey of network interdiction models and algorithms. *European Journal of Operational Research*, 283(3):797–811.

- Xin, S., Wang, X., Zhang, J., Zhou, K., and Chen, Y. (2023). A comparative study of factor graph optimization-based and extended kalman filter-based ppp-b2b/ins integrated navigation. *Remote Sensing*, 15(21):5144.
- Ye, X., Fishkind, D. E., Abrams, L., and Priebe, C. E. (2011). Sensor information monotonicity in disambiguation protocols. *Journal of the Operational Research Society*, 62(1):142–151.
- Ye, X. and Priebe, C. E. (2010). A graph-search based navigation algorithm for traversing a potentially hazardous area with disambiguation. *International Journal of Operations Research and Information Systems (IJORIS)*, 1(3):14–27.
- Yildirim, S., Aksakalli, V., and Alkaya, A. F. (2019). Canadian traveler problem with neutralizations. *Expert Syst. Appl.*, 132:151–165.
- Zweig, A., Ahmed, N., Willke, T. L., and Ma, G. (2020). Neural algorithms for graph navigation. In *Learning Meets Combinatorial Algorithms at NeurIPS2020*.